The Canadian Mineralogist
Vol. 43, pp. 1811-1838 (2005)

XANES SPECTROSCOPY OF SULFUR IN EARTH MATERIALS

MICHAEL E. FLEET[§]

Department of Earth Sciences, University of Western Ontario, London, Ontario N6A 5B7, Canada

ABSTRACT

X-ray absorption near-edge structure (XANES) spectroscopy is the ideal non-destructive technique for characterizing and quantifying S species in compositionally complex natural materials such as silicate glasses and minerals, coals, asphalts and asphaltenes, kerogens and humic substances. Sulfur absorption edges represent the transition of S 1*s* and 2*p* core electrons to unoccupied antibonding orbitals at the bottom of the conduction band. Shifts in the position of the absorption-edge feature of S *K*- and *L*-edge XANES spectra constitute a chemical ruler for oxidation state of both inorganic and organic species of S; the S *K* edge shifts from 2469.5 eV for chalcopyrite (2– oxidation state) to 2482 eV for gypsum (6+). However, chemical state of S in Earth materials is most readily assigned by comparing the overall XANES profile with spectra for reference compounds. Sulfur XANES spectra are reviewed for pyrite, troilite, pyrrhotite and NiAs-type $Co_{0.923}S$ and $Ni_{0.923}S$, niningerite (MgS), oldhamite (CaS), alabandite (MnS) and cubic FeS, and sphalerite and related phases, as well as for selected solid-solutions of the monosulfides. Sulfur XANES spectra for FeS, CoS, NiS, MgS, CaS, MnS and ZnS have been simulated by multiple scattering calculations. The S *K*-edge XANES of transition-metal-bearing monosulfides generally show anomalous absorption consistent with hybridization of the final S 3*p* σ* antibonding states with empty 3*d* orbitals on the metal atoms. Various applications of S *K*- and *L*-edge XANES fingerprinting are discussed, including speciation of inorganic S in basaltic glasses, lazurite and haüyne, identification of organic functional groups of S in coals, kerogens and humic substances extracted from subtropical soils and marine sediments, and the association of sulfated sugars with calcification of coral aragonite skeletons.

Keywords: XANES spectroscopy, chemical state of S, electronic structure and bonding, sulfides, sulfates, magma, organic geochemistry.

SOMMAIRE

La spectroscopie d'absorption des rayons X dans la région pré-seuil (XANES) s'avère la technique non-destructive par excellence pour caractériser et quantifier les espèces de soufre dans les matériaux naturels de composition complexe, par exemple les verres silicatés et minéraux, charbons, asphaltes et asphaltènes, kérogènes et substances humiques. Les seuils d'absorption du soufre résultent de la transition des électrons 1*s* et 2*p* du noyau à des orbites non occupés anti-liaisons à la base de la bande de conduction. Les décalages dans la position des seuils *K* et *L* du soufre des spectres XANES constituent un barème chimique important dans l'évaluation du niveau d'oxydation du soufre, à la fois pour les espèces inorganiques et organiques; le seuil *K* est déplacé de 2469.5 eV dans la chalcopyrite (valence 2–) à 2482 eV dans le gypse (6+). Toutefois, l'état du soufre des matériaux terrestres est plus facilement attribué en comparant le profil XANES entier d'un échantillon aux spectres des composés de référence. Les spectres XANES du soufre sont passés sous revue pour les phases suivantes: pyrite, troïlite, pyrrhotite et $Co_{0.923}S$ et $Ni_{0.923}S$ structuralement de type NiAs, niningerite (MgS), oldhamite (CaS), alabandite (MnS) et FeS cubique, ainsi que sphalérite et phases semblables, de même que ceux des compositions choisies de solutions solides monosulfurées. Les spectres XANES de FeS, CoS, NiS, MgS, CaS, MnS et ZnS ont été simulés par calculs de la dispersion multiple. Le seuil *K* du soufre des monosulfures contenant des métaux de transition montre en général une absorption anormale attribuable à l'hybridisation des états finaux des anti-liaisons 3*p* σ* avec les orbites vides 3*d* des atomes métalliques. Les applications diverses des spectres XANES des seuils *K* et *L* du soufre pour fins d'identification sont ensuite évaluées, par exemple pour déterminer la spéciation du soufre inorganique dans les verres basaltiques, la lazurite et la haüyne, pour identifier les groupes fonctionnels organiques du soufre dans les charbons, kérogènes et substances humiques extraites des sols subtropicaux et des sédiments marins, et pour étudier le lien entre les glucoses sulfatées et la calcification de squelettes d'aragonite dans les coraux.

(Traduit par la Rédaction)

Mots-clés: spectroscopie XANES, état chimique du soufre, structure electronique, liaisons, sulfures, sulfates, magma, géochimie organique.

§ *E-mail address*: mfleet@uwo.ca

Introduction

Sulfur is characteristically heterovalent, exhibiting by far the greatest range in oxidation state (2– to 6+) of the geochemically abundant elements, and readily forms chemical bonds with both more electropositive and more electronegative elements. In consequence, it has a diverse geochemical affinity and is highly mobile under both magmatic and surficial conditions, moving freely among the lithosphere, hydrosphere and atmosphere. Sulfur is an important major to minor constituent in the solar system, having a cosmic atomic abundance close to that of Fe. The average chondrite contains about 1.9 wt% S, and CI carbonaceous chondrite, about 6.2 wt% S, with S occurring almost exclusively as troilite (FeS), although the cubic monosulfides oldhamite (CaS) and niningerite [(Mg,Fe)S] are the important sulfides in rare reduced enstatite chondrites (*e.g.*, Skinner & Luce 1971, Fleet & MacRae 1987). Although S is a candidate for the light-element component in the outer (liquid) core of Earth, it has a very low abundance in the Earth's mantle. Nevertheless, it is an important minor component in magmatic systems, occurring as species dissolved in the silicate melt and vapor phase and as sulfide or sulfate minerals. Sulfur is lost from magmas by the segregation or precipitation of metal sulfides in the upper crust and degassing under near-surface conditions. As reviewed in Fleet *et al.* (2005a), the behavior of S in melts, minerals and fluids is complicated, with speciation changing primarily as a function of composition and fugacity of O and S: in reduced systems, the dissolution of S in magmas is strongly dependent on Fe and less dependent on $f(O_2)$, whereas in oxidized systems, it is strongly dependent on $f(O_2)$. Sulfate becomes important in oxidized wet magmas and is the stable species in surficial environments in open contact with the atmosphere. Interestingly, up to half of the free O of photosynthetic origin produced and removed from the atmosphere throughout Earth history may be sequestered in sedimentary sulfate minerals (*e.g.*, Schidlowski 1981), S redox being up to eight times more efficient than oxidation of ferrous iron in this respect.

The inorganic S species encountered in geochemistry and mineralogy include sulfide (S^{2-}), bisulfide (HS^-), disulfide (S_2^{2-}), other polysulfides (S_n^{1-}, S_n^{2-}), native S (S^0), thiosulfate ($S_2O_3^{2-}$), sulfite (SO_3^{2-}) and sulfate (SO_4^{2-}). Under reducing conditions, S behaves as an anion (or alloying element), forming bonds directly with metal cations, whereas under oxidizing conditions, it is a complex-forming cation, and in some compounds of intermediate oxidation state, it occurs in both anionic and cationic forms. Moreover, organically bound S may be a significant component of the total S of sedimentary rocks, sediments and soils, occurring in fossil fuels, kerogen, humus and microbes. Gaseous forms of S in nature include H_2S and SO_2 (both highly toxic), as well as S_2 at magmatic temperatures. Metal sulfide and disulfide minerals have interesting solid-state properties and are actively studied in solid-state chemistry and mineral physics. These minerals belong to the broad spectrum of metal chalcogenide compounds that crystallize with familiar structure-types, such as those of nickeline, pyrite, marcasite, sphalerite, wurtzite and halite; they have numerous applications in the high-technology industrial sector.

This paper is a review of the application of S *K*- and *L*-edge X-ray absorption near-edge structure (XANES) spectroscopy in mineralogy and geochemistry. XANES spectroscopy has proven to be the ideal *in situ* and non-destructive technique for studying the chemical state of S in Earth materials. The XANES spectrum is a fingerprint of chemical state, equivalent in many respects to the X-ray powder-diffraction pattern of standard crystalline materials. Sulfur *K*- and *L*-edge XANES spectra have been used to characterize and quantify S in compositionally complex natural materials such as silicate glasses, silicate and phosphate minerals, coal, petroleum and related hydrocarbons and humic substances, as well as in metal sulfides and sulfates. Moreover, XANES spectra yield insight into the chemical bonding of S in minerals, with the promise of more fundamental information as the theoretical background of XANES evolves. The fiftieth anniversary of The Mineralogical Association of Canada coincides with the general availability of Canadian Light Source (CLS) beamlines to the user community. It is appropriate to focus this review on S XANES because Canadian researchers have been prominent in developing X-ray absorption spectroscopy (XAS) in the soft and ultrasoft X-ray regions as an investigative tool in mineralogy and geochemistry, and S is a critical element in the formation and exploitation of metalliferous ore deposits and energy resources.

Overview of Theory and Practise

X-ray absorption spectroscopy (XAS) is concerned with analysis of the fine structure in the X-ray absorption profile. For energies below about 10 keV, X-rays are absorbed by photo-ionization, a process in which a photon is absorbed by an atom and an electron is excited to a bound or quasi-bound state. The absorption coefficient in this energy region decreases discontinuously, in a characteristic sawtooth pattern, with increasing energy of X-ray photons or decreasing wavelength (λ). The discontinuities, or *absorption edges*, correspond to the threshold energies of the allowed photoelectron transitions from core-electron orbital levels of the constituent atoms to the lowest unoccupied orbital levels above the valence band, and are restricted by the atomic selection rules $\Delta L = \pm 1$, $\Delta J = 0$ or ± 1, where ΔL and ΔJ represent change in the quantum numbers for total orbital angular momentum (L) and grand total angular momentum (J). The photoelectron transition channels important in S XANES are summarized in Figure 1. For the halite-structure monosulfide MgS

(niningerite), which is an insulator and does not have 3*d* electrons, the final states are unoccupied antibonding orbitals at the bottom of the conduction band. Thus, an edge jump at ~2475 eV in the X-ray absorption profile of MgS represents the S *K* edge and corresponds to the photoelectron transition S $1s \rightarrow$ S $3p$ σ^*, and a composite edge-jump near 163–164 eV represents the S *L* edge and corresponds to the photoelectron transition S $2p \rightarrow$ S $3s$ σ^*. In addition, transition to empty S 3*d* states may result in a second absorption peak in the ultrasoft X-ray region at somewhat higher energy. Complications arise for certain transition-metal sulfides, like pyrrhotite, where the *K* edge represents transition to unoccupied S $3p$ σ^* states hybridized with empty Fe 3*d* states. More generally, final states for photoelectron transitions may also include empty *d* bands and π orbitals (*e.g.*, Fleet & Muthupari 2000), as well as unoccupied π^* antibonding orbitals, with the first two resulting in sharp pre-peaks in absorption spectra. The photoelectron transition defining the S *K* edge most commonly results in a recognizable peak, or *white line* (*e.g.*, Figs. 2, 3), located slightly above the Fermi level (E_F) and ionization threshold.

Absorption fine-structure occurs in the vicinity of the edge, extending to about 200 eV above the edge for light elements and 1000 eV for heavy elements. It is conventionally divided into two regions: XANES, which extends from the threshold for absorption to about 25–40 eV above the edge, and EXAFS (extended X-ray absorption fine structure), which extends to higher energies. XANES theory and applications were reviewed in Durham (1988) and Bianconi (1988), and foundation papers include Kutzler *et al*. (1980), Natoli *et al*. (1980), Stöhr *et al*. (1983) and Bunker & Stern (1984). EXAFS spectra are characterized by an oscillation superimposed on an otherwise monotonically decreasing profile that falls off with λ^3 dependency. Its basic physical explanation (modulation of the outgoing photoelectron wave by back-scattering from neighboring atoms) has been known for some time (*e.g.*, Lytle *et al*. 1975, Stern 1988). Fourier transform

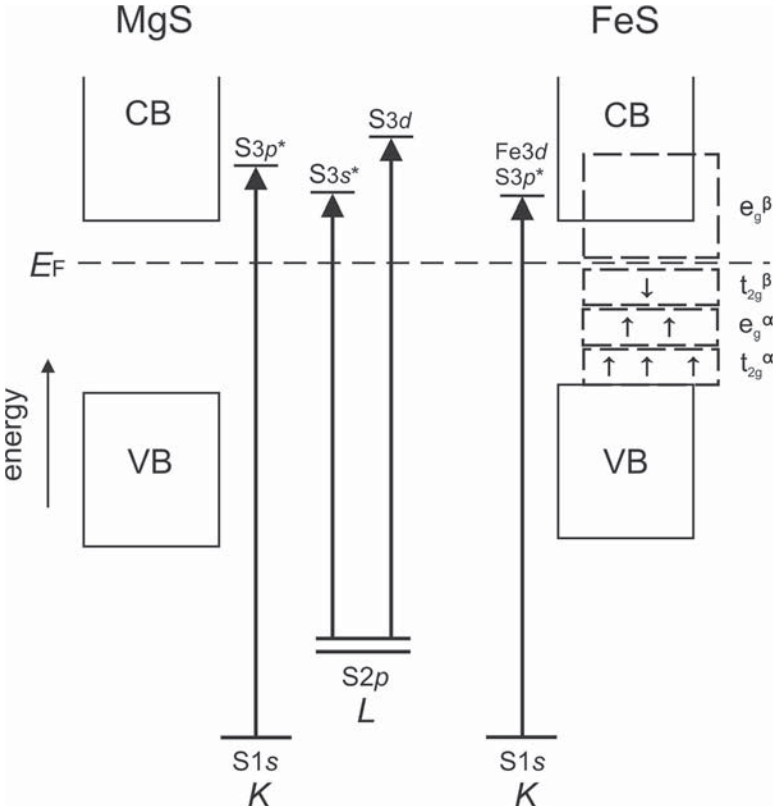

FIG. 1. Schematic band-structure models for halite-type MgS (niningerite) and derivative NiAs-type FeS (troilite), showing photoelectron transitions associated with S *K* and *L* absorption edges. Here, VB is valence band, CB is conduction band, α indicates majority (↑) 3*d* electron states, β indicates minority (↓) 3*d* states, and E_F is the Fermi level.

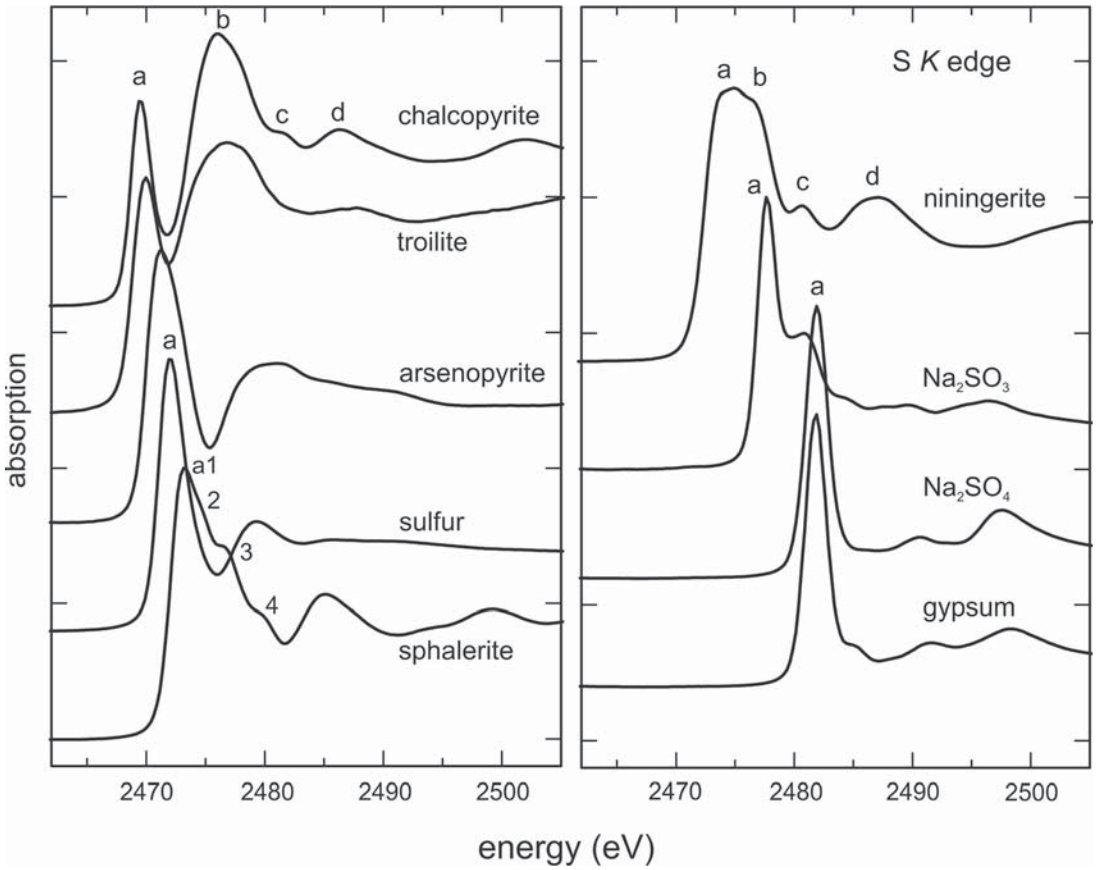

FIG. 2. Sulfur *K*-edge XANES spectra for some reference compounds and minerals, showing, in both left and right panels, the progressive shift of the absorption-edge peak (**a**) to higher energy with increase in oxidation state of S. Troilite is $Fe_{0.923}S$, and close in composition to hexagonal pyrrhotite; niningerite is the MgS end-member. The spectra were collected in total electron yield (TEY) mode.

of the EXAFS spectrum yields information on bond distance(s), coordination number and thermal + static displacement of the absorber atom. EXAFS is a unique probe of the local environment of atoms in condensed matter. Unfortunately, for atoms of low atomic number, absorption fine-structure decays rapidly past the edge, so that the information that EXAFS can provide for light elements like S is limited (*e.g.*, Bunker & Stern 1984).

On the other hand, XANES spectra for light elements are relatively animated, and have provided information on oxidation states of S and B (Li *et al.* 1995a, 1996), nearest-neighbor coordination of B, Al and Si (Fleet & Muthupari 2000, Li *et al.* 1995b, c, Fleet *et al.* 1997) and differential bonding in borate and borosilicate minerals (Fleet & Liu 2001). Moreover, the strength of absorption peaks is proportional to the amount of absorber species present. This relation is quantitative for S *K*-edge XANES spectra of metal–sulfide solid-solutions (Farrell & Fleet 2000, 2001, Farrell *et al.* 2002), minor amounts of S species in coals (Hussain *et al.* 1982, Huffman *et al.* 1991), and minor to trace amounts of S in basaltic glass (Paris *et al.* 2001, Fleet *et al.* 2005a). Because both initial and final electron states are important in defining the transition energy associated with the edge feature, the XANES spectrum yields information on the lower part of the conduction band, and the chemical state and local stereochemical environment of the absorber atom. Moreover, through hybridization of unoccupied antibonding orbitals and empty metal 3*d* orbitals of S, S *K*- and *L*-edge XANES spectra also reveal details of the 3*d* electron configuration and bonding of metal atoms coordinated with S, even though the metal atoms are not probed directly. The XANES spectrum is, in fact, a map of the unoccupied partial density-of-states (DOS) above the valence band of the analyzed compound, as viewed through the perspective of the absorber atom.

Where the unoccupied partial DOS can be interpreted using a molecular orbital diagram or energy band and DOS calculation (and also with data for electrical and magnetic properties), S XANES provide insight into the electronic structure of S-bearing minerals. Finally, S *K*- and *L*-edge XANES spectra are reproducible, from one measurement to another, and are becoming increasingly more important for fingerprinting S moieties in complex natural materials.

Disappointingly, it is still not possible to extract bond distances and details of local coordination from XANES spectra of uncharacterized materials, but there have been encouraging advances in the simulation of S *K*- and $L_{2,3}$-edge XANES of alkaline-earth and transition-metal monosulfides using multiple-scattering theory (Durham 1988, Bianconi 1988, Farrell *et al*. 2002, Soldatov *et al*. 2004). The EXAFS oscillation is the product of a single scattering process extending into $\boldsymbol{k}$ space. In this form, the EXAFS spectrum can be Fourier-transformed to yield a radial distribution function in real space. The nature of the XANES spectrum is much more complex, involving the photoelectron transition at the edge and modulation of the transition energy by multiple scattering pathways above the edge. Therefore, it is not amenable to Fourier transformation (or any other form of inversion). The separation of the XANES and EXAFS regions is also obscure. Bianconi (1988) suggested that the boundary between the two spectral regions could be considered to be where the wave vector of the photoelectron ($\boldsymbol{k}$) equals $2\pi/R$ (R is the shortest interatomic distance): in the XANES region, the photoelectron wavelength is greater than the interatomic distance ($\boldsymbol{k} < 2\pi/R$), and multiple scattering dominates. However, systematic shifts of the σ-shape resonances in

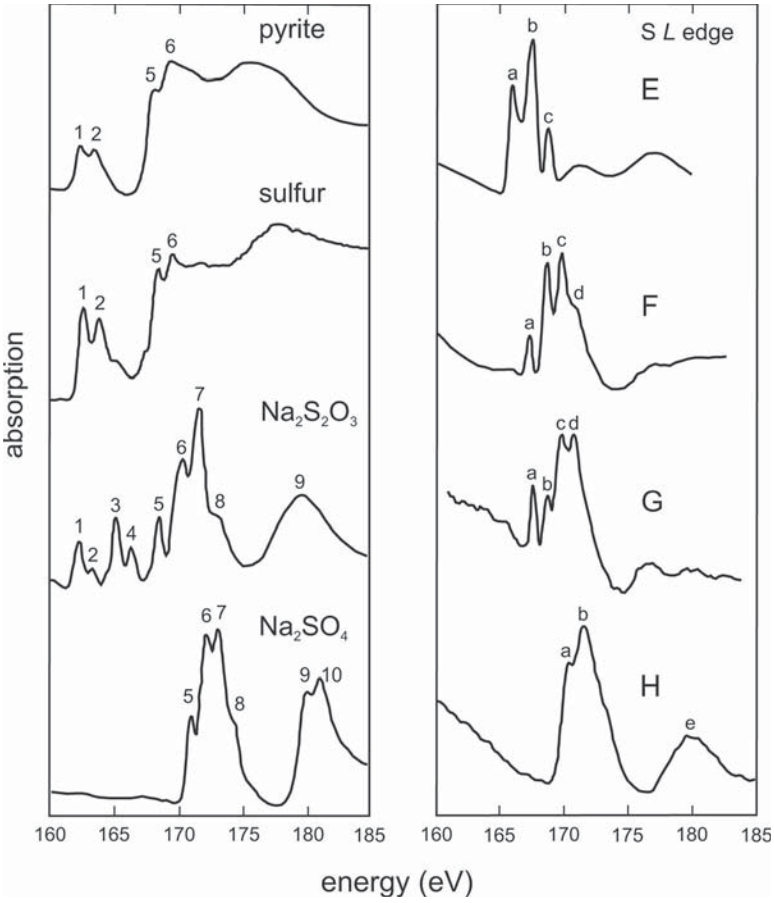

FIG. 3. Sulfur *L*-edge XANES spectra for some reference compounds, including pyrite, native S, sodium thiosulfate, sodium sulfate, (E) DL-methionine sulfoxide, (F) dibenzothiophene sulfone, (G) poly(1,4-phenelene ether-sulfone) and (H) sodium anthraquinone-2-sulfonic acid (after Kasrai *et al*. 1996b).

the absorption spectra of gas-phase molecules (Stöhr *et al*. 1983, Sette *et al*. 1984) and of peaks in the XANES spectra of cubic sulfides and halides (Kasrai *et al*. 1988, 1991) suggest that single scattering extends well into the XANES region. The shifts in these spectral features are consistent with Natoli's rule (*e.g*., Stern 1988) which states that the energy of an absorption peak above the threshold, ΔE, is inversely proportional to R^2, where R is either a lattice spacing or interatomic distance, giving $(\Delta E\, R^2) = C$; C is a constant for the absorbing material, equal to 150.4 eVÅ^2 for the free electron, and the $1/R^2$ dependence is identified with the basic EXAFS expression. The linear correlation for the S *L*-edge XANES spectrum of galena (PbS) extends downward to about 11 eV above the threshold (Fig. 4).

The XANES spectra of UWO researchers discussed presently were collected at the Canadian Synchrotron Radiation Facility (CSRF), Aladdin storage ring (University of Wisconsin at Madison, Wisconsin). The beamlines used are described in Yang *et al*. (1992), Bancroft (1992) and Tan *et al*. (1982), and typical experimental procedures are summarized in Farrell *et al*. (2002) and Fleet *et al*. (2005c). For the most part, these XANES spectra have been energy-calibrated to the S *K*- and L_3-edge features of native S at 2472.0 and 162.5 eV, respectively (Fuggle & Inglesfield 1992), although some earlier studies used slightly different values, and some spectra have been calibrated against pyrite. The S *K* and *L* edges lie in the soft and ultrasoft X-ray regions, respectively, requiring very low-pressure conditions (~10^{-9} Torr) for their measurement. Unlike silicate minerals and strongly bonded insulating materials in general, considerable care has to be taken in sample preparation for sulfides, because metal sulfides are reactive to air, and the resulting oxidation and hydration at the mineral surface and near-surface are greatly enhanced by crushing and grinding. Sulfur *K*- and *L*-edge XANES recorded by total electron yield (TEY, or current yield) are essentially near-surface measurements: the sample depths probed are estimated to be ~230 Å and <50 Å for TEY, compared with 1000–2000 Å and >600 Å for fluorescence yield (FY), respectively (Kawai *et al*. 1994, Kasrai *et al*. 1996a). Sample preparation for S *L*-edge XANES should be made in a glove bag filled with dry nitrogen gas and attached to the sample port of the spectrometer (Farrell *et al*. 2002, Kravtsova *et al*. 2004), and for S *K*-edge XANES, exposure to air and crushing of the sample should be minimal. It is desirable to make simultaneous measurements of TEY and FY to ensure that the signal from the near surface corresponds to that from the bulk. The surfaces of monosulfides of the 3*d* transition metals (*e.g*., $Ti_{1-x}S$, $Fe_{1-x}S$, $Co_{1-x}S$ and $Ni_{1-x}S$) and pyrite-group CoS_2 and NiS_2 are particularly reactive to air. The Co and Ni sulfides readily oxidize to sulfates in the near-surface, and published S *K*-edge XANES of these compounds commonly show a spurious peak near 2482 eV, corresponding to the *K* edge of sulfate; *e.g*., see discussion of Zajdel *et al*. (1999) in Farrell & Fleet (2001). Also, a spurious sulfate peak in XANES spectra of synthetic and basaltic S-bearing glass is not uncommon, and is most readily attributable to near-surface oxidation of reduced S species during sample preparation (Fleet *et al*. 2005a).

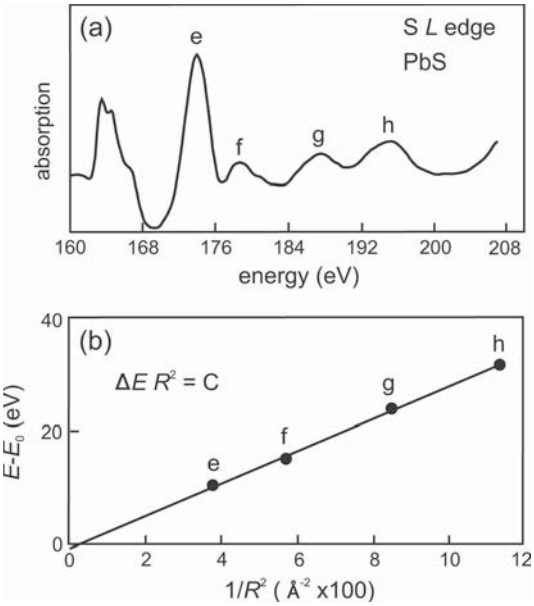

FIG. 4. (a) Background-subtracted S *L*-edge XANES spectrum for galena, and (b) correlation plot between energy above threshold (ΔE) and $1/R^2$ for peaks **h** (nearest-neighbor shell; S–Pb interaction), **g** (lattice spacing; d_{111}), **f** (second shell; S–S), and **e** (third shell; S–Pb) (after Kasrai *et al*. 1991).

TABLE 1. POSITION OF S *K*- AND L_3-EDGE PEAKS IN SOME MINERALS AND COMPOUNDS

Mineral or Compound	*K* edge energy (eV)	L_3 edge energy (eV)	Mineral or Compound	*K* edge energy (eV)	L_3 edge energy (eV)
chalcopyrite	2469.5	160.4	arsenopyrite	2471.2	-
α-$Ni_{0.923}S$	2469.7	160.7	pyrite	2471.5	162.3
troilite ($Fe_{0.923}S$)	2470.0	160.4[1]	native S	2472.0	162.5
pyrrhotite	2470.0	160.5[1]	$Na_2S_2O_3$	2471.4 2480.2	162.2 170.2
sphalerite	2473.3	164.0	Na_2SO_3	2477.8	168.0
wurtzite	2473.5	-	Na_2SO_4	2481.9	170.8
oldhamite (CaS)	2474.0 2477.4	163.1 -	$CaSO_4 \cdot 2H_2O$	2481.9	171.1
niningerite (MgS)	2475.1	164.3	gypsum	2481.9	-

[1] second L_3-edge peak at 161.4 eV.

Chemical Shift of S *K* and $L_{2,3}$ Edges and Oxidation State of Sulfur

Numerous studies have shown that synchrotron radiation XANES spectroscopy is a sensitive probe of the local structure and chemical state of S in minerals and chemical compounds (*e.g.*, Hitchcock *et al*. 1987, Kitamura *et al*. 1988, Vairavamurthy *et al*. 1993a, b, Li *et al*. 1995a, Womes *et al*. 1997, Vairavamurthy 1998, Farrell & Fleet 2000, 2001, Farrell *et al*. 2002, Paris *et al*. 2001, Kravtsova *et al*. 2004, Fleet *et al*. 2005a, b). Representative *K*- and $L_{2,3}$-edge XANES spectra for some minerals and synthetic compounds of known composition and structural or molecular state (reference compounds) are given in Figures 2 and 3, respectively. The *K*-edge spectra are characterized by a prominent absorption-edge feature **a**, attributable to transition of the S 1*s* core electron to the lowest unoccupied antibonding states on the S atom, and various post-edge features **b**, **c**, **d**, *etc*., attributable largely to multiple-scattering resonances, with the broad feature **b** in the XANES spectrum of $Fe_{0.923}S$ having contributions from both sources. For most of these reference compounds (*e.g.*, niningerite, native S, Na_2SO_3 and gypsum), the bottom of the conduction band is populated by S 3*s* σ* and S 3*p* σ* orbitals, and the *K*-edge feature represents the photoelectron transition S 1*s* → S 3*p* σ*, the 1*s* → 3*s* transition channel being forbidden by the atomic selection rules. Complications arise for sulfides with low-lying empty 3*d* orbitals (transition-metal sulfides and CaS) owing to hybridization of S antibonding states and metal 3*d* states (*e.g.*, Farrell & Fleet 2001, Farrell *et al*. 2002, Kravtsova *et al*. 2004, Soldatov *et al*. 2004). The positions of the edge peak of XANES spectra represent the characteristic chemical shifts, and are reproducible to ±0.1 eV (Table 1). Li *et al*. (1995a) and others have demonstrated a progressive shift of the S *K* and $L_{2,3}$ absorption edges to higher energy with increase in the oxidation state of S, spanning 10–12 eV from sulfides (2–) to native S (0), sulfite (4+) and sulfate (6+). The energy position of the edge feature of S *K*-edge XANES increases from 2469.5–2470 eV for transition-metal monosulfides (2–) to 2471 eV for disulfides of the pyrite group (1–), 2472 eV for native S (0), 2478 eV for sulfites and 2482 eV for sulfates (Fig. 5).

This ruler for the chemical state of S works well for metallic sulfides, native S and oxysulfides, but is complicated by an overall shift of about 45 eV in the positions of *K*- and *L*-edge peaks for metal sulfides (all of nominal 2– oxidation state for S), which vary from 2469.5 and 160.4 eV for chalcopyrite to 2475.1 and

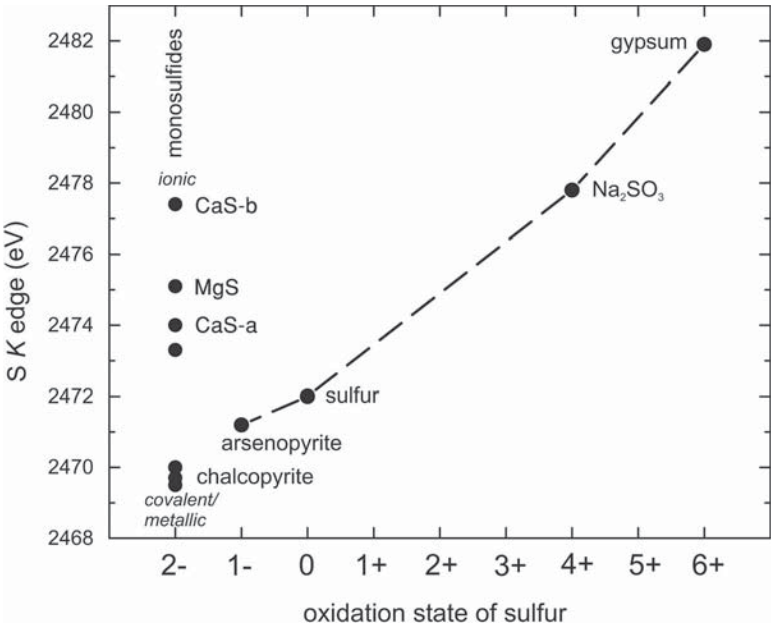

FIG. 5. Position of S *K* edge for some reference compounds and minerals, showing a curvilinear correlation with oxidation state of S for compositions ranging from metallic metal sulfides to gypsum. Note also the marked influence of bond character of monosulfides, with the *K* edge shifting to higher energy with decreasing covalence (after Fleet *et al*. 2005a).

164.3 eV for niningerite, respectively (Table 1), and correlate linearly with increase in the direct energy-band gap (Li *et al*. 1994a). Fleet *et al*. (2005a) noted that the nature of the metal exerts a considerable influence on the position of the absorption edges of the metal sulfides because, in these structures, the S atom is bonded directly to the metal cation. In respect to physical properties, these minerals and compounds span the full range from metals, to small band-gap covalently bound semiconductors, to ionic insulators. As the position of the absorption edge is determined very largely by the final state of the photoelectron (at the bottom of the conduction band), it is clear that the edge peak must shift to higher energy as the band gap opens up. The variation in S *K*-edge position from 2469.5 eV for chalcopyrite to 2477 eV for the second edge-peak of oldhamite (CaS), all representing the nominal 2– oxidation state, spans the full range of reduced and intermediate oxidation states of S species in the chemical-shift scale shown in Figure 5, from S^{2-} to S^{4+}. For this reason, the overall XANES profile of reference compounds (the XANES fingerprint) is often much more useful than the actual edge-position for assignment of oxidation state and speciation of S in complex Earth materials.

Sulfides

S K-edge XANES

The S *K*-edge XANES spectra for synthetic Fe, Co and Ni monosulfides with the hexagonal NiAs-type (nickeline-type, B8) structure are superficially similar (Fig. 6), differing principally in the size of the edge peak **a**. As noted above, this edge feature (white line) is commonly attributed to the $s \rightarrow (p,d)$ transition channel (see also Pong *et al*. 1994, Womes *et al*. 1997). Although transition of a 1*s* core electron to unoccupied 3*d* nonbonding and antibonding states is forbidden by the atomic selection rules in the electric-dipole approximation ($L = \pm 1$), these forbidden transitions become weakly to strongly allowed at both the metal and S *K* edges of metal sulfides through hybridization of S antibonding and metal 3*d* states (*e.g*., Tossell 1977). This *p–d* hybridization is particularly strong for $3d(e_g)$ states of octahedrally coordinated metal atoms. Peak **a** is also referred to elsewhere as a "pre-edge" feature, but recent studies suggest that it is indeed located above the Fermi level (E_F) at the bottom of the conduction band. For example, Womes *et al*. (1997) calculated the band structures of synthetic troilite (FeS) and pyrite (FeS_2), including the S 3*s* and 3*p* and Fe 3*d*, 4*s* and 4*p* states, using the tight-binding approach, and compared the partial density-of-states (PDOS) at the bottom of the conduction band with their experimental XANES spectra (Fig. 7). XANES measurements were made at the S *K* and Fe *K* and L_3 edges for both of these Fe sulfides, and the XANES and PDOS were compared on a common energy-scale using calculated values of E_F. The vertical dashed lines in Figure 7 locate maxima in the PDOS and indicate possible schemes of hybridization. Womes *et al*. (1997) assigned peak **a** in the S *K*-edge XANES of troilite (FeS), as above, to transition to S 3*p* σ* states mixed with unoccupied Fe 3*d* states, and the broad feature **b** to transitions to S *p*-like states in the conduction band hybridized with Fe 4*sp* orbitals, but noted that the intensity of this latter peak (**b**) may be intensified by multiple-scattering effects in the continuum. On the other hand, the Fe 3*d* and S 3*p* σ* states in pyrite are separated by about 0.7 eV. In consequence, mixing of the Fe 3*d* and S 3*p* states is more limited, and the S *K*-edge peak is defined largely by transition to S 3*p* σ* states. The onset of the second, broad feature in the S *K*-edge XANES of pyrite represents transition to S 3*p* states hybridized with Fe 4*s* and 4*p* states.

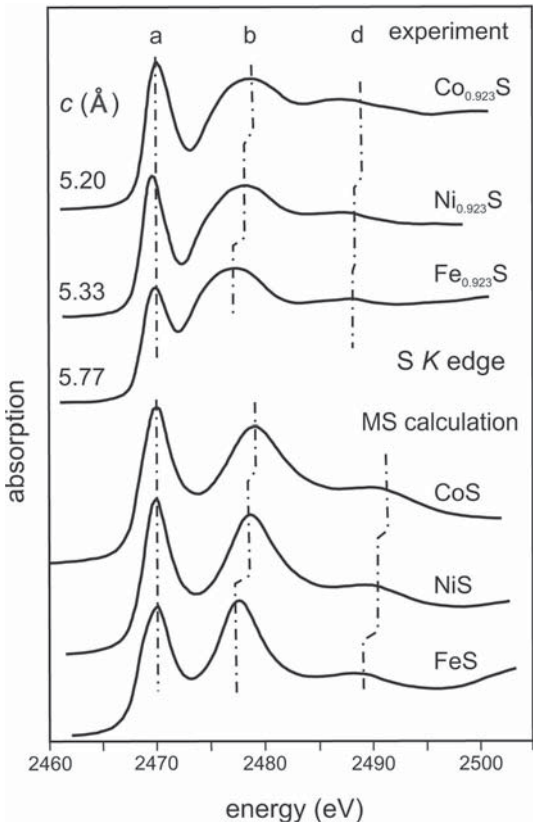

FIG. 6. Sulfur *K*-edge XANES spectra for synthetic NiAs-type $Fe_{0.923}S$, $Co_{0.923}S$ and $Ni_{0.923}S$, compared with *c* spacing in the hexagonal unit-cell and corresponding simulated spectra for FeS, CoS and NiS, calculated using the multiple-scattering (MS) program G4XANES for a cluster size of four neighbor shells (37 atoms) in the ground-state potential (after Soldatov *et al*. 2004).

As reviewed in Farrell & Fleet (2001), the 3*d* electron configurations of the divalent Fe, Co and Ni monosulfides with the NiAs-type or -derivative structure are well understood from the magnetic behavior of these compounds (*e.g.*, Hobbs & Hafner 1999). Stoichiometric FeS is antiferromagnetic at room temperature (*RT*; *i.e.*, the mineral troilite; see Fig. 1), but paramagnetic above 420 K, whereas at *RT*, pyrrhotite is variously paramagnetic, antiferromagnetic and ferrimagnetic with progressive increase in Fe vacancies. Ferrous iron in these monosulfides has the high spin $t_{2g}^4 - e_g^2$ configuration with the majority spin (↑) t_{2g}^{α} and e_g^{α} bands filled, minority spin (↓) t_{2g}^{β} band one-third filled, and minority spin (↓) e_g^{β} band empty. On the other hand, $Co_{1-x}S$ is Pauli paramagnetic at *RT*, and divalent Co has the low spin $t_{2g}^6 - e_g^1$ electronic configuration, with majority spin (↑) t_{2g}^{α} and minority spin (↓) t_{2g}^{β} bands filled, majority spin (↑) e_g^{α} band half-filled and minority spin (↓) e_g^{β} band empty. Moreover, α-NiS is paramagnetic at *RT* and antiferromagnetic below 260 K, and divalent Ni has the high spin $t_{2g}^6 - e_g^2$ configuration, with majority spin (↑) t_{2g}^{α} and e_g^{α} and minority spin (↓) t_{2g}^{β} bands filled, and minority spin (↓) e_g^{β} band empty.

Stoichiometric FeS (troilite) is a small-band-gap semiconductor, but the nature of this band gap and of the metallic behavior above 420 K is controversial, because electron delocalization through overlap of the half-filled t_{2g}^{β} and empty e_g^{β} bands is prohibited by symmetry. Goodenough (1967) recognized that trigonal distortion of the face-shared FeS_6 octahedra below 420 *K* could split the t_{2g} levels into narrow bands parallel

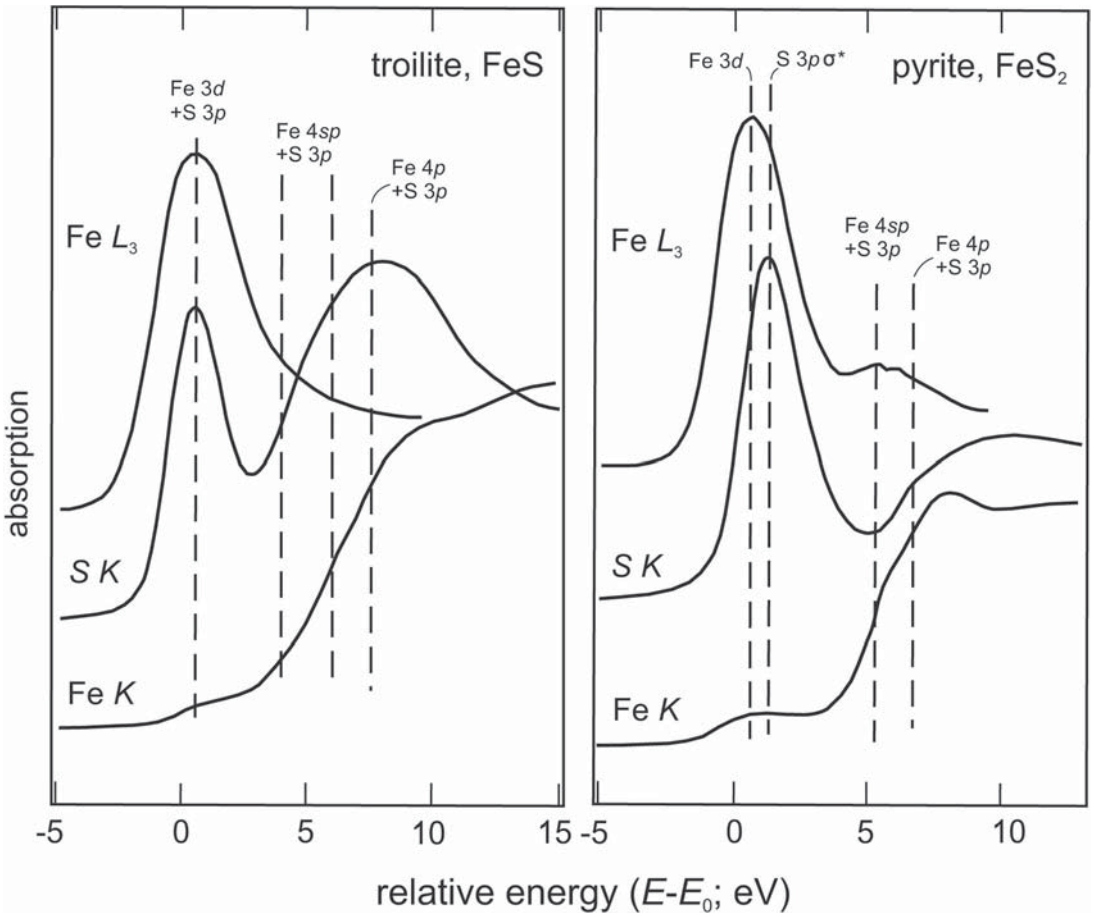

FIG. 7. Superposition of the S *K*- and Fe *K*- and L_3-edge XANES and theoretical partial density-of-states (DOS) on a common (relative) energy-scale, for pyrite and troilite (FeS); vertical dashed lines locate maxima in partial DOS, and their alignment with spectral features suggests possible hybridization schemes for the final states of photoelectron transitions (after Womes *et al.* 1997).

(Γ_I) and normal (Γ_{II}) to the *c* axis, and thus directly account for the energy gap; partial overlap of the Γ_I and Γ_{II} bands at the transition temperature would explain the metallic behavior at higher temperature. However, recent density-of-states (DOS) studies invoke extensive hybrization of S 3*p* and metal 3*d* states in the valence band and attribute the metallic behavior to metal–S–metal π bonding (*e.g.*, Raybaud *et al.* 1997). Metallic behavior in $Co_{1-x}S$ and NiS is generally attributed to delocalization of e_g^{α} electrons through overlap of the e_g^{α} and e_g^{β} bands. Although the nature of the chemical bonding and metal–metal interaction in transition-metal chalcogenides and pnictides with the NiAs-type and derivative structures remains controversial (*e.g.*, Marfunin 1979, Sakkopoulos *et al.* 1984, 1986, Dijkstra *et al.* 1989, Tossell & Vaughan 1992, Nakamura *et al.* 1993, Raybaud *et al.* 1997, Hobbs & Hafner 1999), most studies show that, at the metal-rich limit of the Fe, Co and Ni monosulfides, the metallic character increases in the sequence FeS < NiS < $Co_{1-x}S$, and is associated with progressive increase in covalence and decrease in metal 3*d* electron-interaction energy.

The size of the edge peak for the S *K*-edge XANES spectra in Figure 6 is, to a first approximation, proportional to the number of available final states and, hence, to the extent of hybridization of empty S 3*p* σ^* antibonding and metal 3*d*(e_g) orbitals (Pong *et al.* 1994). Unoccupied e_g^{β} states have the appropriate symmetry for hybridization with *p* states (*e.g.*, Farrell & Fleet 2001), although other authors also recognize a contribution from metal t_{2g} states in NiAs-type sulfides (*e.g.*, Womes *et al.* 1997). Given the availability of empty e_g^{β} states, the second critical factor controlling the area of the edge peak is the degree of covalence of the metal–S bonds, which increases with increase in metallic character. Briefly, an increase in metallic character is associated with decrease in unit-cell volume and shorter metal–S bonds, and thus, increase in covalence and orbital (or band) overlap (*e.g.*, Nakamura *et al.* 1993). The progressive increase in area of the edge peak in the sequence $Co_{1-x}S > Ni_{1-x}S > Fe_{1-x}S$ is in complete agreement with data on the unit-cell volumes (values of *c* unit-cell parameter are given in Fig. 6) and band-energy models for these monosulfides.

Farrell & Fleet (2001) also measured the variation in edge-peak area of the S *K*-edge XANES spectra for synthetic binary and ternary solid-solutions in the system $Fe_{0.923}S$ – $Co_{0.923}S$ – $Ni_{0.923}S$ (Fig. 8); the nonstoichiometric composition was adopted to avoid precipitation of a Co-rich pentlandite phase. Farrell & Fleet made the interesting observation that the area of the edge peak does not correlate directly with average number of 3*d* electrons per metal atom. The plots of edge-peak area *versus* binary composition have a maximum value at the end-member $Co_{0.923}S$, but not at other combinations of metal atoms giving a 3*d* electron count of 6.83 (which is the average number of 3*d* electrons per Co atom in $Co_{0.923}S$). The lowest values of edge-peak area occur for $Fe_{0.923}S$ – $Ni_{0.923}S$ binary compositions, and the ternary compositions have intermediate values. Although the absorber atom is S, the final states available to the photoelectron are determined by the nearest-neighbor metal atoms. Hence, the absorption of synchrotron radiation is modulated by the local electronic structure of individual absorber atoms, rather than by the average band-structure of the crystals. This distinction between local and crystal phenomena is related to the time scale of the measurement and, in particular, the short relaxation-times of transitions involving core electrons. Furthermore, because edge-peak area directly reflects increase in the number and availability of empty e_g orbitals and covalence of metal–S bonds, the correlation between edge-peak area and metallic character for NiAs-type Fe–Co–Ni monosulfides is graphic experimental evidence for hybridization of S antibonding and metal 3*d* orbitals.

In recent work, S *K*- and $L_{2,3}$-edge XANES for synthetic $Fe_{0.923}S$, $Co_{0.923}S$ and $Ni_{0.923}S$ were measured and simulated using a full multiple-scattering (MS) approach and assuming ideal formulae for FeS, CoS and NiS, respectively (Soldatov *et al.* 2004). The S *K*-edge results are shown in Figure 6. The multiple-scattering simulations were made with the computer code G4XANES (Della Longa *et al.* 1995), and the FEFF8.2 computing package (Ankudinov *et al.* 1998) was used to calculate the local densities-of-states (DOS). The

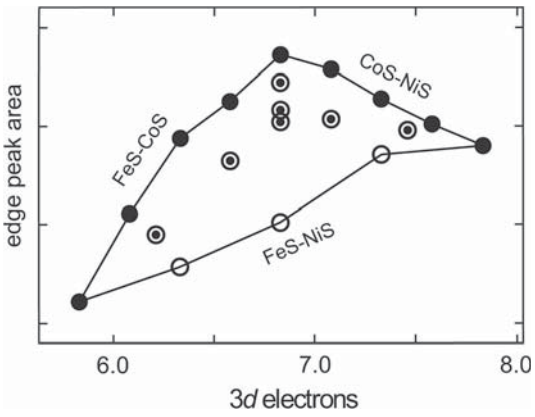

FIG. 8. Area of edge peak in the S *K*-edge XANES spectra for binary and ternary Fe–Co–Ni monosulfides [$(Fe,Co,Ni)_{0.923}S$] compared with the average number of 3*d* electrons per metal atom. Full circles are binary $(Fe,Co)_{0.923}S$ and $(Co,Ni)_{0.923}S$ solid-solutions, open circles are binary $(Fe,Ni)_{0.923}S$ solid-solutions, and centered circles are ternary solid-solutions. Note that the maximum peak-area occurs at $Co_{0.923}S$ rather than at 6.83 3*d* electrons, showing that absorption of synchrotron radiation is related to local electronic structure of individual absorber atoms, rather than a group (crystal band) effect (after Farrell & Fleet 2001).

calculated XANES show good agreement with the experimental spectra, for both edges and for relatively small atomic clusters, *i.e.*, 19 to 37 atoms, with the latter size of cluster corresponding to four neighbor shells. One evident shortcoming in the results for the S *K*-edge XANES is that feature **b** is more peaked in the calculated spectra. However, the simulations do show the progressive increase in strength of the edge peak **a** and shift of features **b** and **c** to higher energy in the sequence FeS to NiS and CoS (least metallic to most metallic). The latter result is in agreement with Natoli's rule (Bianconi 1988), which states that for solids of the same structure-type, the energy position of XANES peaks above the threshold (ΔE) is inversely proportional to interatomic distance or lattice spacing (R). The application of Natoli's rule to the XANES spectra of simple cubic structures (Kasrai *et al*. 1991) has been noted above. The calculated local partial spin-polarized density of unoccupied electron states for these compounds (Kravtsova *et al*. 2004, Soldatov *et al*. 2004) resulted in similar distributions for the separate spin-up and spin-down states. More interestingly, in addition to the "normal" hybridization of admixture type (where the maximum of one partial DOS corresponds to the maximum of another), there is a second type of hybridization in which the density of S *p* states is pushed away from the interval of metal *d* states. The results for NiS (Fig. 9) show that over a narrow region of energy immediately *below* E_F, the interaction between occupied S *p* states and Ni *d* states has a repulsive character. This conclusion is consistent with the calculated energy-band structures of transition-metal compounds, which tend to restrict the metal *d* states to narrow bands above the valence band.

The S *K*- and $L_{2,3}$-edge XANES spectra of synthetic end-members and binary solid-solutions of monosulfides having the cubic rocksalt (B1) structure-type in the system CaS–MgS–MnS–FeS were investigated by Farrell & Fleet (2000), Farrell *et al*. (2002) and Kravtsova *et al*. (2004), who also calculated the partial DOS in the conduction band of MgS and CaS, and troilite as well. The composition space investigated includes oldhamite (CaS), alabandite (MnS) and niningerite [(Mg,Fe)S]. At the temperature of synthesis (1000°C), solid solution is complete along the MgS–MnS join, and extends to 68 and 74 mol.% FeS along the MgS–FeS and MgS–MnS joins, respectively (Skinner & Luce 1971). Representative S *K*-edge XANES are shown in Figure 10. At room temperature and pressure, both MgS and CaS are diamagnetic and classical insulators or large indirect band-gap semiconductors. The band gap (2.7 eV) in niningerite (MgS) is bounded by S 3*p* bonding orbitals in the upper part of the valence band and unoccupied Mg 3*s* (and to a lesser extent, S 3*d*) orbitals and S 3*p* σ* antibonding orbitals in the lower part of the conduction band. The bottom of the conduction band of oldhamite (CaS) is complex and crowded by unoccupied Ca 3*d* orbitals and Ca 4*s* and S 3*p* σ* antibonding orbitals. Alabandite (MnS) is a diluted magnetic semiconductor and reportedly has exceptional magnetic and magneto-optical properties derived through interaction of hybridized S *sp* and Mn 3*d* states (Sato *et al*. 1997). At room temperature, α-MnS has an antiferromagnetic spin-ordered structure with the high-spin t_{2g}^3 and e_g^2 configuration. The band gap lies between occupied Mn 3*d* states in the valence band and unoccupied S 3*p* σ* antibonding states hybridized with empty Mn 3$d(e_g)$ and 3$d(t_{2g})$ states in the conduction band.

In agreement with these electronic structures, the S *K*-edge of niningerite (MgS) shows no evidence of *p*–*d* hybridization, but the $s \rightarrow (p,d)$ transition channel is represented by the first (broad) peak **a1** of the compound edge feature of oldhamite (CaS) and the shoulder **a** on the edge feature of alabandite (MnS) (Fig. 10). The splitting of the S *K*-edge feature of CaS due to the $s \rightarrow (p,d)$ transition channel is nicely reproduced by the multiple-scattering simulation of Farrell *et al*. (2002) (Fig. 11). These calculations were made in the ground-state potential of the absorber atom, although the relaxed state of the atom, which takes into account the presence of the core hole created by the electronic transition, is thought to be a more appropriate physical model. The latter is readily approximated by using the electronic structure of the element of adjacent (higher) atomic number, the so-called $Z + 1$ approximation (Bianconi 1988). As Figure 11 shows, there is no significant difference between the relaxed- and excited-state spectra for oldhamite (CaS). More systematic simulations of the S *K*- and $L_{2,3}$-edge XANES spectra for the cubic monosulfides are given in Kravtsova *et al*. (2004), who

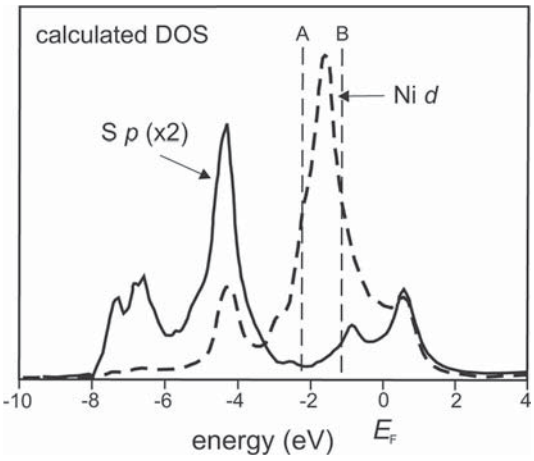

FIG. 9. The Ni *d* and S *p* densities of electronic states (DOS) in the valence band of NiS, calculated for a cluster size of 170 atoms. The S *p* DOS is multiplied by a factor of two; note that S *p* states "avoid" Ni *d* states in the interval A–B (after Soldatov *et al*. 2004).

noted that agreement with corresponding experimental spectra required comparatively large atomic clusters of 9 to 13 neighbor shells.

The experimental S *K*-edge XANES spectra for the cubic solid-solutions show progressive evolution of a satellite shoulder or peak on the low-energy flank of the edge feature **a** (Fig. 12), which for the Fe-bearing sulfides is aligned with the edge peak of cubic FeS (B1) (Fig. 10) and represents progressively increasing participation of metal 3*d* orbitals in metal–S bonding with increase in substitution by Fe in (Mg,Fe)S and (Mn,Fe)S and by Mn in (Mg,Mn)S (Farrell & Fleet 2000, Farrell *et al*. 2002). Increase in satellite-peak area reflects an increase in overall attainability of metal 3*d* states for hybridization with S 3*p* σ* antibonding states as proportionally more metal 3*d* orbitals become available. Note that the area of the satellite peak does not increase linearly, as would be expected from a simple mixing of cations, showing that real changes in bulk electronic properties have occurred. Interestingly, the inflections in the satellite peak-area distributions for (Mn,Fe)S and (Mg,Fe)S (Fig. 12) are in precise agreement with the phase boundaries determined from X-ray powder diffraction (Skinner & Luce 1971, McCammon *et al*. 1984), the two-phase regions being [alabandite + FeS (B8)] and [niningerite + FeS (B8)], respectively.

There have been several studies of X-ray absorption in synthetic solid-solutions with the sphalerite (B3) and wurtzite structures, which have metal and S atoms in tetrahedral coordination (Li *et al*. 1994b, Pong *et al*. 1994, Ławniczak-Jabłonska *et al*. 1996). The systems investigated include $Zn_{1-x}Fe_xS$ to $x = 0.40$, at the S *K* and *L* edges (Li *et al*. 1994b), $Zn_{1-x}M_xS$ (M = Mn,Fe,Co) to x(Mn) = 0.6, x(Fe,Co) = 0.5, at the Zn $L_{2,3}$ edge ($Zn_{1-x}Mn_xS$ only) and S *K* edge (Pong *et al*. 1994), and $Zn_{1-x}M_xS$ (M = Mn,Fe,Co,Ni) to x(Mn) = 0.33, x(Fe) = 0.50, x(Co) = 0.25 and x(Ni) = 0.01, and $Zn_{1-x}M_xSe$ to x(Mn) = 0.37, x(Fe) = 0.18, x(Co) = 0.07 and x(Ni) = 0.01, at the *K* edges of all cations and anions (Ławniczak-Jabłonska *et al*. 1996). The *K*-edge XANES of the metals with incompletely filled 3*d* orbitals (Mn,

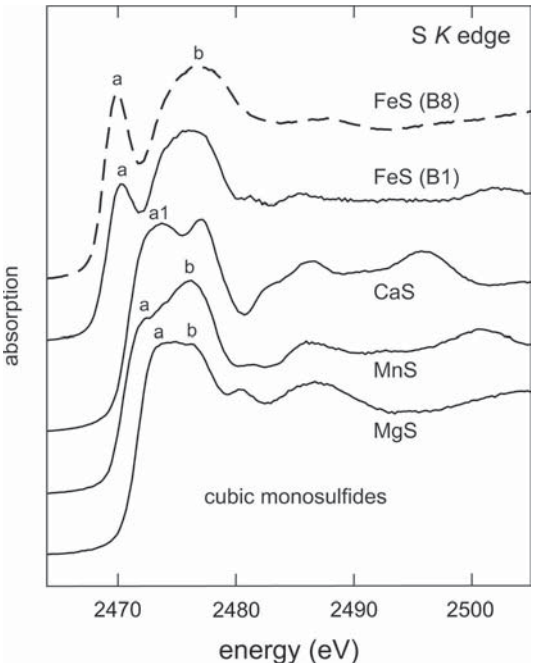

FIG. 10. Sulfur *K*-edge XANES spectra for rocksalt (B1) structure FeS, oldhamite (CaS), alabandite (MnS) and niningerite (MgS), compared with spectrum for troilite (FeS); spectra were recorded by fluorescence yield (after Farrell *et al*. 2002).

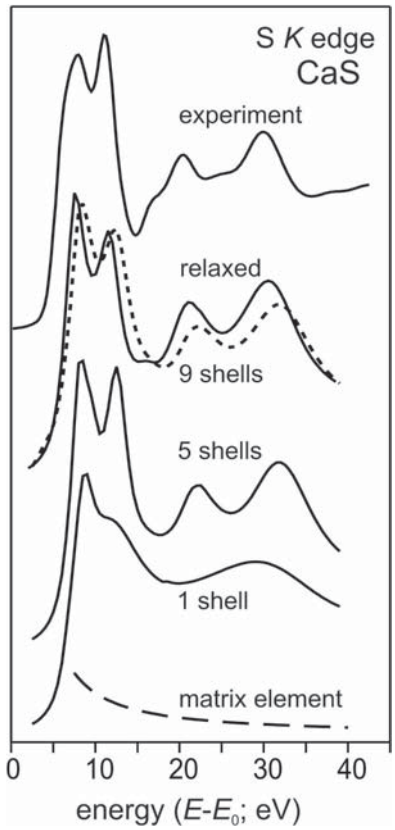

FIG. 11. Sulfur *K*-edge XANES for oldhamite (CaS) calculated using multiple-scattering theory in the ground-state potential. Note that a good agreement with the experimental spectrum requires a large-size cluster of nine neighbor shells, and the Z + 1 approximation (relaxed, dashed spectrum) does not result in a significant improvement (after Farrell *et al*. 2002).

Fe, Co and Ni) all show a weak pre-edge feature, attributable to the transition channel *TM* 1*s* → *TM* 3*d* (where *TM* is transition metal), which is forbidden in the dipole approximation, but becomes weakly to strongly allowed through distortion of the tetrahedral sites of the metals. In addition, the S *K*-edge XANES of the tetrahedral sulfides $Zn_{1-x}Fe_xS$ and $Zn_{1-x}Co_xS$ show progressive evolution of a low-energy satellite shoulder to the edge feature **a1** of the ZnS spectrum (Fig. 2) with increase in substitution by Fe and Co (a similar feature was present but not noted in Li *et al*. 1994b). This low-energy satellite shoulder was assigned to transition of S 1*s* electrons to unoccupied hybridized S 3*p* σ* (or S 3*s*,*p* σ*) antibonding and empty metal 3*d*(t_2) states. By analogy to the cubic monosulfide solid-solutions (above), this shoulder corresponds to the edge feature of hypothetical end-member tetrahedral FeS and CoS, and represents progressively increasing participation of metal 3*d* orbitals in the metal–S bonding.

The edge feature of the S *K*-edge XANES spectrum of sphalerite (ZnS) has a stepped appearance, with all researchers (Sainctavit *et al*. 1987, Li *et al*. 1994b, Pong *et al*. 1994, Ławniczak-Jabłonska *et al*. 1996) recognizing four peaks or shoulders of progressively diminishing intensity (*e.g*., Fig. 2). This characteristic absorption profile was reproduced in an early X-alpha multiple-scattering simulation (Sainctavit *et al*. 1987). The S *K*-edge XANES of wurtzite (hexagonal ZnS) is essentially identical to that of sphalerite for similar bulk-compositions, and the edge feature becomes more peaked in the sequence sphalerite or wurtzite, greenockite (wurtzite-structure CdS) or hawleyite (sphalerite-structure CdS), metacinnabar (sphalerite-structure HgS) and cinnabar (trigonal-structure HgS), with **a1** dominating as the white line at the edge and **a3** subordinate in cinnabar and metacinnabar (Li *et al*. 1994b). The positions of the S *K*- and *L*-edge features also shift to lower energy, by about 2 eV, through this series of monosulfides, the S *K*- and L_3-edge values in Li *et al*. (1995a) being 2473.4 and 163.6 for sphalerite, 2473.2 and 163.5 for wurtzite, 2472.3 and 162.2 for greenockite, 2471.7 and 162.0 for metacinnabar and 2471.1 eV and 161.8 eV for cinnabar, relative to 2472.0 eV and 162.7 eV for native S, respectively. Sulfur is in fourfold (tetrahedral) coordination in the sphalerite- and wurtzite-structure monosulfides, but in cinnabar it has only two nearest-neighbor Hg atoms. Li *et al*. (1994b) also pointed out that the Cl *K*-edge XANES of CuCl and the P *K*-edge XANES of InP are strikingly similar to the S *K*-edge XANES of sphalerite. This agreement amongst compounds of the same structure-type (sphalerite) but dissimilar chemical composition is a clear demonstration of the control of local geometry and electronic configuration of the absorber atom on the form of the XANES spectrum.

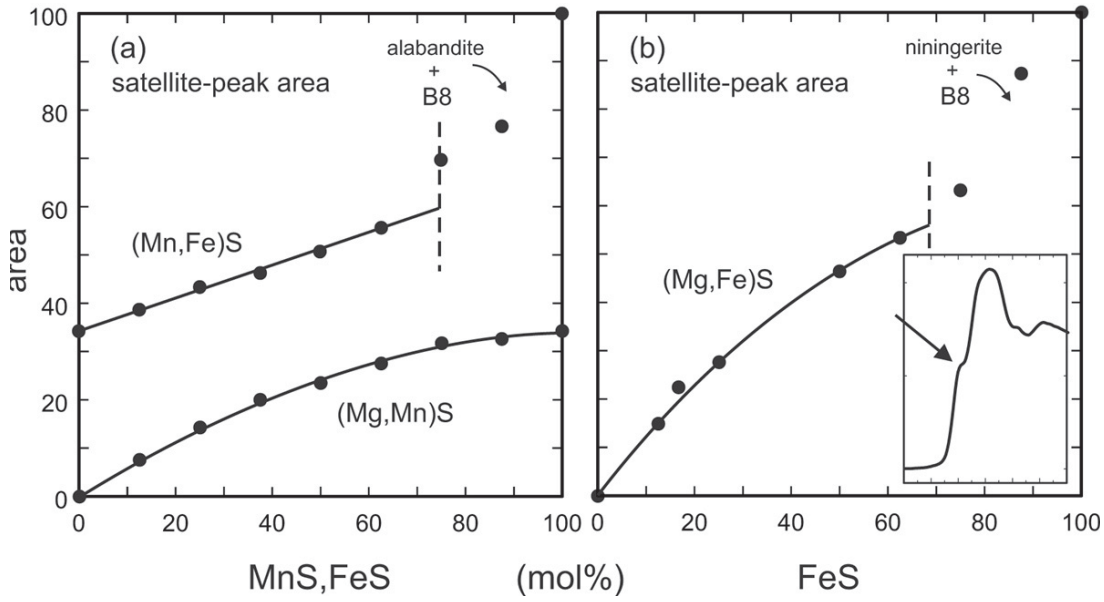

FIG. 12. Dependence of satellite-peak area on bulk composition, for S *K*-edge XANES spectra of (a) (Mn,Fe)S and (Mg,Mn)S, and (b) (Mg,Fe)S solid-solutions. The inset locates the satellite on the low-energy flank of the edge peak for $(Mg_{0.37}Fe_{0.63})S$. The smooth increase in satellite-peak area with composition is interpreted to represent progressive increase in unoccupied metal 3*d*(e_g^{β}) DOS. Inflections indicate phase boundaries, in good agreement with powder XRD determinations (after Farrell *et al*. 2002).

S L-edge XANES spectra

The S $L_{2,3}$-edge XANES spectra have proven less useful than the *K*-edge XANES for understanding the partially unoccupied DOS in the conduction band of sulfides, because of their surface sensitivity and complexity. The edge features of S *L*-edge XANES spectra for the ferrous-metal monosulfides, for example, tend to be diffuse and weakly developed above background, even where stringent precautions are taken to exclude contamination by air. Representative S *L*-edge spectra are reported in Li *et al*. (1995a) for pyrrhotite, pyrite, carrollite, $MgSO_4$•$2H_2O$, gypsum, anhydrite, celestine and barite, Kasrai *et al*. (1996b; present Fig. 3) for pyrite, native S, $Na_2S_2O_3$, Na_2SO_4 and various organic S compounds), Farrell *et al*. (2002) for niningerite, oldhamite, alabandite, troilite, native S and the cubic-monosulfide solid-solutions, Kravtsova *et al*. (2004) for experimental and multiple scattering simulations of MgS, CaS, MnS and troilite, and Soldatov *et al*. (2004) for experimental and multiple-scattering simulations of $Fe_{0.923}S$, $Co_{0.923}S$ and $Ni_{0.923}S$). In addition, there is an extensive review of S *L*-edge XANES spectra for metal sulfides in Chen (1997).

All assignments of excitations for S *L*-edge XANES of metal sulfides have emphasized the importance of hybridization of S and metal orbitals. The S *L* edge represents transition of S 2*p* core-level electrons to unoccupied molecular-orbital states (S 3*s* σ*, S 3*d*, metal 3*d*, *etc*.), as permitted by the atomic-selection rules. The absorption edge is split by spin–orbit interaction, resulting in two separate edges (L_3 and L_2) overlapped and separated by 1.1–1.2 eV. In the absence of hybridization, the L_3 and L_2 edges represent the photoelectron transitions S $2p_{2/3} \rightarrow$ S 3*s* σ* and $2p_{1/2} \rightarrow$ S 3*s* σ*, respectively, which result in an ideal L_3:L_2 peak area ratio close to 2:1. The L_3- and L_2-edge peaks in the spectrum for native S (Fig. 3) are presently labeled **1** and **2**, respectively. This spectrum is well resolved and reproducible, even though native S is volatile at the very low pressure in the spectrometer. The S *L*-edge XANES spectrum for pyrite (and marcasite) is not unlike that for native S (Fig. 3), with well-resolved L_3,L_2 edge peaks, and is seemingly dominated by contributions from the covalently bound disulfide ion. This is somewhat surprising because, in pyrite and marcasite, S is in tetrahedral coordination to one S and three Fe atoms.

In contrast, the edge peaks in the S *L*-edge XANES for $Fe_{1-x}S$ (and of NiAs-type $Co_{0.923}S$ and $Ni_{0.923}S$, as well) are weak (Soldatov *et al*. 2004), and resolution of the separate L_3,L_2 edges is dependent on sample preparation and measurement procedures. Hybridization of unoccupied S 3*s* σ* antibonding orbitals and empty metal 3*d* orbitals further complicates the S *L*-edge XANES of the 3*d* transition-metal sulfides. For NiAs-type-structure $Fe_{1-x}S$, the L_3 edge peak now represents a transition to S 3*s* σ* states hybridized with Fe 3*d* states, and L_2 to transition to S 3*s* σ* states hybridized with Fe $3d(e_g)$ states. The diffuse edge-feature in the spectrum for FeS was described as a pre-edge peak in Farrell *et al*. (2002) because it is displaced to lower energy, but this displacement is better interpreted simply as the chemical shift expected for a small-band-gap semiconducting monosulfide (*cf*. Table 1). Although $Co_{0.923}S$ and $Ni_{0.923}S$ both gave spectra with the typical doublet (L_3,L_2) edge feature, the S *L*-edge feature of $Fe_{1-x}S$ consists of three peaks, at 160.4, 161.4 and 162.4 eV for synthetic troilite ($Fe_{0.923}S$) and 160.5, 161.4 and 162.4 eV for a crystal of pyrrhotite (Table 1). This triplet edge-feature is consistent with two overlapped L_3,L_2 edges, and possibly represents crystal-field splitting of the final state S 3s σ* antibonding orbitals hybridized with empty Fe 3*d* orbitals. Crystal-field splitting of the conduction-band DOS is well documented for the S *L*-edge XANES spectrum of CdI_2 type, van-der-Waals-bonded TiS_2 (Chen 1997), resulting, in this case, in an initial set of spin-orbit split peaks about 2.5 eV below the main L_3,L_2 edge feature. Titanium has a formal $3d^0$ configuration in TiS_2, which allows for extensive hybridization of empty metal 3*d* orbitals with unoccupied S 3*s* σ* and 3*p* σ* antibonding orbitals. Thus, the S *K*-edge feature of TiS_2 is also split by the crystal field into two peaks of nearly equal intensity (Wu *et al*. 1997, Fleet *et al*. 2005c), and is fairly well reproduced by multiple-scattering calculations (Wu *et al*. 1997, Bocharov *et al*. 1998). The edge features of the S *L*-edge XANES spectra for niningerite (MgS) and oldhamite (CaS) are strong (Farrell *et al*. 2002), but remain difficult to assign in terms of simple L_3,L_2 doublets, even after fairly rigorous theoretical study (Kravtsova *et al*. 2004).

Oxyanions of Sulfur

Sulfur in intermediate and 6+ oxidation states forms a large number of complex anions with O, although perhaps only thiosulfate, sulfite and sulfate, along with SO_2, sulfurous and sulfuric acid, are of significance in mineralogy and geochemistry. The coordination of S atoms in these oxyanions varies from one (the terminal thiosulfide atom), to three and four in tetrahedral $S(SO_3)$ and SO_4. The S *K*- and *L*-edge spectra (Figs. 2, 13, 14; Li *et al*. 1995a, Kasrai *et al*. 1996b) exhibit a progressive increase in the energy position of the edge feature with increase in oxidation state, reflecting the progressive increase in charge on the absorber atom, to maximum values of 2482 eV and about 171 eV, respectively, for divalent metal sulfates, although Paris *et al*. (2001) reported a value of 2483.1 eV for the *K*-edge peak of sulfate in a natural apatite. In Figure 13, which is after Li *et al*. (1995a), the *K* and *L* edges of the sulfates $MgSO_4$•$2H_2O$, gypsum ($CaSO_4$•$2H_2O$), anhydrite, celestine and barite are correlated on a common energy-scale using the S $K\alpha_1$ X-ray emission energy at 2307.8 eV and the S 1*s* binding energy for *K*-edge spectra and the S $2p_{3/2}$ binding energy for *L*-edge

spectra. These composite *K*- and *L*-edge spectra give a qualitative picture of the unoccupied DOS at the bottom of the conduction band. Li *et al*. (1995a) assigned the *K* edge of the sulfates (peak C) to the photoelectron transition S $1s \rightarrow 3p$-like antibonding states (of the sp^3 tetrahedral hybrid σ bonds). For the *L* edge, peak A was assigned to the transition of S 2*p* electrons to S 3*s*-like states of a_1 symmetry; the edge is split by about 1.2 eV, owing to the spin-orbit interaction of S 2*p* orbitals. Peak E was assigned to transition to S 3*d*-like *e* and t_2 states; this peak is weak in the *K*-edge XANES spectra because the transition channel $1s \rightarrow 3d$ is forbidden in the dipole approximation.

The XANES spectra, and especially the S *L*-edge XANES, of the oxyanions tend to be complex and little understood. The spectra are generally composite, representing the superposition of absorption edges associated with different functional S atoms (and different S–S and S–O bonds), as well as separate L_3 and L_2 edges in *L*-edge spectra. They are, however, entirely reproducible from one measurement to another, making possible the reliable fingerprinting of small amounts of S-oxyanion salts in complex amorphous materials (*e.g*., Kasrai *et al*. 1996a). The strong peaks in S *K*-edge spectra generally correspond to the absorption-edge peaks of the different functional S atoms, and can be identified using the chemical-shift ruler of Figure 5. A single sharp peak at 2482 eV in the S *K*-edge XANES is characteristic of sulfate; for example, Fleet *et al*. (2005a) recorded a value of 2481.9 eV for the edge-peak of each of gypsum, analytical reagent $CaSO_4 \bullet 2H_2O$ and Na_2SO_4 (peak **4** in Fig. 14, Table 1). Also, peaks **1** and **4** in the S *K*-edge XANES of the thiosulfates at 2471.4 and 2480.2 eV, respectively (Fig. 14), broadly correspond to the *K*-edge peaks of the thio (S^{2-}) and sulfate (S^{6+}) atoms in these salts. The meta-bisulfite ion has the assym-

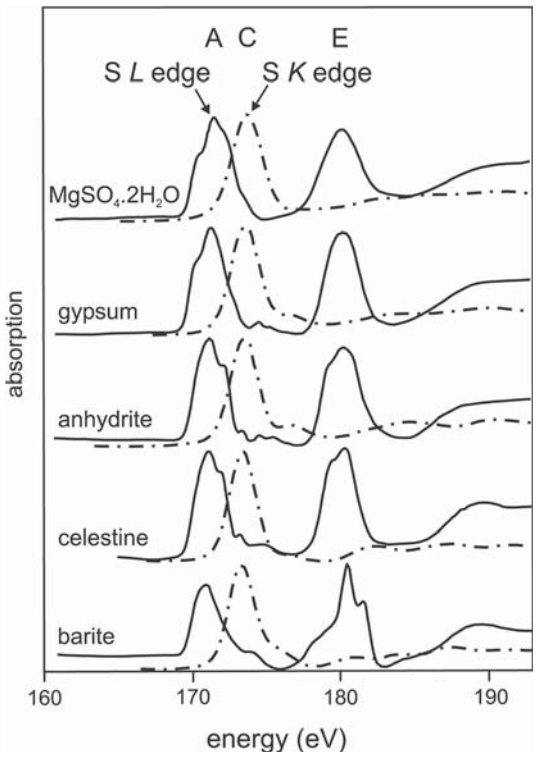

FIG. 13. Sulfur *K*- (dashed curves) and *L*-edge XANES spectra for synthetic $MgSO_4 \bullet 2H_2O$, gypsum, anhydrite, celestine and barite, correlated using the S $K\alpha_1$ X-ray emission energy at 2307.8 eV and the S 1*s* binding energy (BE) for *K*-edge spectra, and the $2p_{3/2}$ BE for *L*-edge spectra. **A** is the S *L*-edge peak, and **C** is the S *K*-edge peak (after Li *et al*. 1995a).

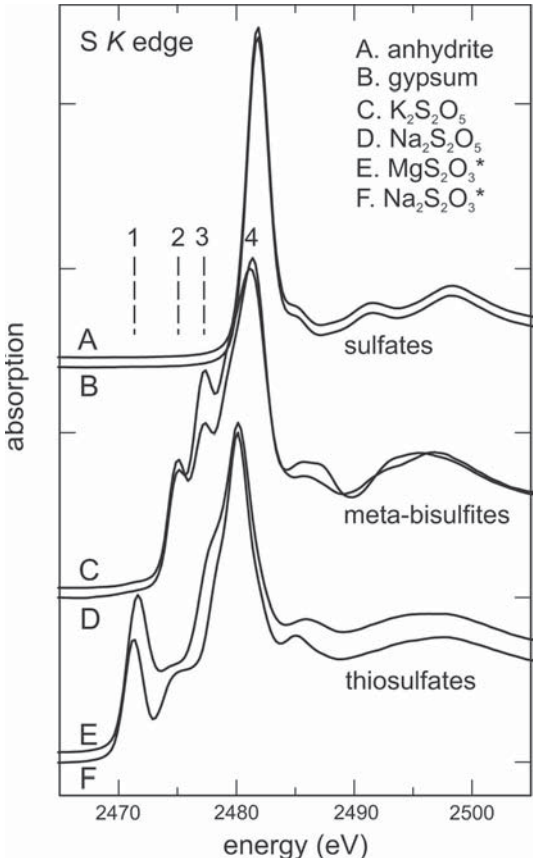

FIG. 14. Sulfur *K*-edge XANES spectra for some S oxyanions, arranged to emphasize the local nature of photoelectron transitions associated with the absorption of X-rays. **1** marks the edge peak for thio S, and **4** the edge peak for S–O bonds of sulfate; note that Na thiosulfate (F) is a pentahydrate, and Mg thiosulfate (E) a hexahydrate.

metrical configuration $[O_2S(1)–S(2)O_3]^{2–}$ in which the two parts of the anion are held together by a rather weak S–S bond (S–S = 2.17 Å, compared with 2.08 Å in pyrite). The loose attachment of the $O_2S(1)$ group is further supported by the mode of formation of the salt $K_2S_2O_5$, which crystallizes by saturating a solution of K_2SO_3 with SO_2. The broad peak **4** in the S *K*-edge XANES spectra of $Na_2S_2O_5$ and $K_2S_2O_5$ (Fig. 14) no doubt corresponds to the edges of the five S^{4+}–O bonds, and the satellite peaks **2** and **3** could represent the edges for transitions associated with the weaker S(1)–S(2) and S(2)–S(1) bonds, respectively.

The spectra for the oxyanion salts of S emphasize the extremely local nature of photoelectron transitions associated with the absorption of X-rays near absorption edges. The XANES spectra are dominated by the chemical composition and geometry of the oxyanions, and are very largely independent of the extended structure of the salts. Thus, in Figure 14, compare the S *K*-edge XANES of Na and Mg thiosulfate (monovalent cation and pentahydrate, and divalent cation and hexahydrate salts, respectively), Na and K meta-bisulfite (medium- to large-sized cation Na, and large-sized cation K salts) and gypsum and anhydrite (dihydrate and anhydrous salts). Similarly, *K*- and *L*-edge XANES for a medium-sized cation dihydrate, a medium- to large-sized cation dihydrate, and several medium- to large- to very-large-sized cation anhydrous sulfates are compared in Figure 13. Note, however, that the S *L*-edge peaks (A) for the dihydrates have a prominent shoulder on the low-energy flank, whereas the anhydrous sulfates have a shoulder of similar intensity on the high-energy flank.

The hydrous sulfates of Ca^{2+} and a broad selection of 3*d* transition-metal cations (including Sc^{3+}, Cr^{3+}, Mn^{2+}, Fe^{3+}, Fe^{2+}, Co^{2+}, Ni^{2+} and Zn^{2+}) have been investigated by S *K*-edge XANES spectroscopy (Okude *et al*. 1999). Many of these spectra exhibit a weak pre-edge feature attributable to crystal-field splitting of S 3*p*-like antibonding orbitals hybridized with empty metal 3*d* orbitals. The energy position of the S *K* edge decreases almost linearly with increase in the number of 3*d* electrons, by about 1 eV from Ca^{2+} to Zn^{2+}.

Silicate Glasses

Paris *et al*. (2001) used S *K*-edge XANES spectroscopy to study the speciation of S in some natural and synthetic glasses of basaltic to rhyolitic compositions and S contents of 0.045 to 0.30 wt.%. Spectra for a back-arc basalt, three samples of dacite from Mt. St. Helens equilibrated in the laboratory at 2–3 kbar and magnetite–hematite (MH) or Mn oxide (MNO) oxygen buffers, and a standard Na–Ca silicate glass equilibrated in air are shown in Figure 15. Sulfide and sulfate were the only S species detected. The S *K*-edge XANES for the basalt is dominated by sulfide, with minor sulfate; dacite No. 59a has more similar amounts of sulfide and sulfate, whereas the spectra for the other two samples of dacite are dominated by sulfate with only a trace of sulfide. As expected, the NBS standard glass made by melting in air shows only sulfate. Taking advantage of the enhanced brightness of a third-generation source at the European Synchrotron Radiation Facility (ESRF; Grenoble) and recent developments in beamline technology, Bonnin-Mosbah *et al*. (2002) and Métrich *et al*. (2002, 2003) obtained S *K*-edge XANES spectra for glass inclusions in olivine from basaltic rocks, selected to cover a range of different volcanic zones and redox conditions, and including ocean-island basalt, back-arc basalt and mid-ocean-ridge basalt. The glass inclusions are about 100 μm in size and have S contents of 0.100 to 0.165 wt.%. The synchrotron beam was focused to 0.3×0.3 μm^2 at the S *K* edge and 2×2 μm^2 at the Fe *K* edge (which also was measured), and the sample was rastered using a piezoelectric device fitted to the sample stage. Although their micro-XANES spectra are dominated by sulfide and sulfate species, a few spectra for glass from oxidized and H_2O-rich basaltic arc

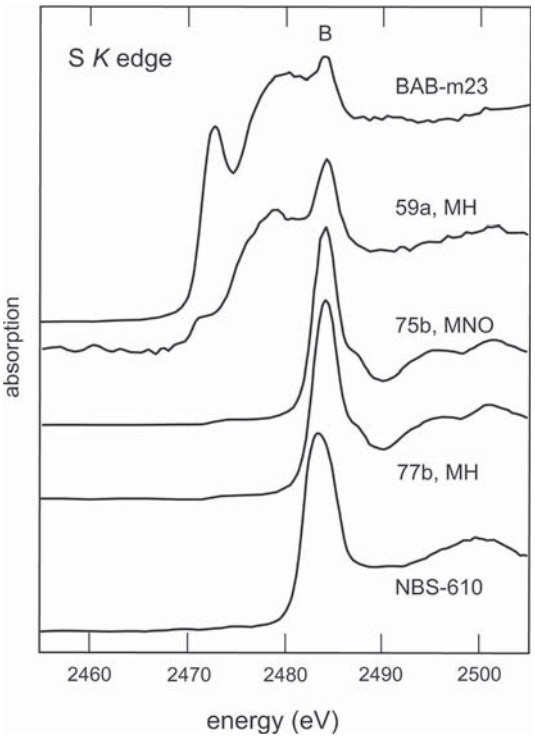

FIG. 15. Sulfur *K*-edge XANES spectra for S-bearing silicate glasses. BAB is a back-arc basalt, 59a, 75b and 77b are dacite samples from Mt. St. Helens, laboratory-equilibrated at magnetite–hematite (MH) and Mn oxide (MNO) solid buffers of oxygen fugacity, and NBS–610 is a standard Na–Ca silicate glass equilibrated in air. The sharp feature B is the edge peak of sulfate (after Paris *et al*. 2001).

volcanoes (Mt. Stromboli) show a weak peak near 2478 eV, corresponding to the S *K* edge of sulfite (Fig. 2). Therefore, Bonnin-Mosbah *et al*. (2002) suggested that S^{4+} (as SO_3^{2-} or SO_2) might occur in natural silicate glasses. In subsequent studies, Métrich *et al*. (2002, 2003) proposed that S^{4+} is the important intermediate species for the degassing of excess S in oxidized and H_2O-rich basaltic arc volcanoes. However, Fleet *et al*. (2005b) also observed a weak peak consistent with a minor to trace amount of sulfite in a S *K*-edge XANES spectrum of scapolite, but cautioned that, where sulfide and sulfate species are present in the bulk sample, sulfite is a possible product of auto-redox reactions at the sample surface (or near surface) during either sample preparation or XANES measurement (see also Smart *et al*. 1999).

Sulfur *K*-edge XANES spectroscopy was used by Fleet *et al*. (2005a) to determine the chemical state and local environment of S in samples of basaltic glass from the eastern Galapagos rift (Perfit *et al*. 1983) and quenched laboratory experiments. An energy-selective fluorescence detector was used for glasses with less than 0.2 wt.% S. Fleet *et al*. (2005a) also investigated S in melts in the system $6NaAlSiO_4$–CaS–$CaSO_4$ quenched from 1500°C. The S *K*-edge XANES spectrum of CaS dissolved in Na-aluminosilicate glass is dominated by a broad singlet edge-feature near 2475 eV (Fig. 16), which more or less corresponds to the first edge-peak in the spectrum of crystalline CaS (oldhamite; Figs. 10, 11). The second peak near 2477 eV in the edge structure of oldhamite is absent in the XANES spectrum of the glass and, thus, seems to be a multiple-scattering feature associated with the extended halite structure. This suggestion is confirmed by Kravtsova *et al*. (2004), who showed that fairly large clusters (consisting of 9- to 13-neighbor shells) of halite-structure CaS are required to simulate the S *K*-edge XANES of oldhamite using multiple-scattering theory (Fig. 11). In contrast, S occurs as isolated SCa_n coordination polyhedra in the glass (and melt) and yields only the first, singlet feature of the S *K*-edge XANES spectrum. The XANES spectrum of $CaSO_4$ dissolved in Na-aluminosilicate glass is dominated by a sharp peak at about 2482 eV, corresponding to the *K* edge of sulfate (S^{6+}; Fig. 16); the extended XANES spectrum is similar to that of crystalline sulfate bonded to Ca^{2+} (*cf*., Figs. 2, 13). Linear correlations between relative XANES area and wt.% content of S were established in Fleet *et al*. (2005a) and used to estimate the content of S in basaltic glasses. The minimum detection-limit for S (*i.e*., resolution of the S *K* edge above background) seems to be significantly less than 100 ppm, although information on the chemical state at this low concentration is very limited.

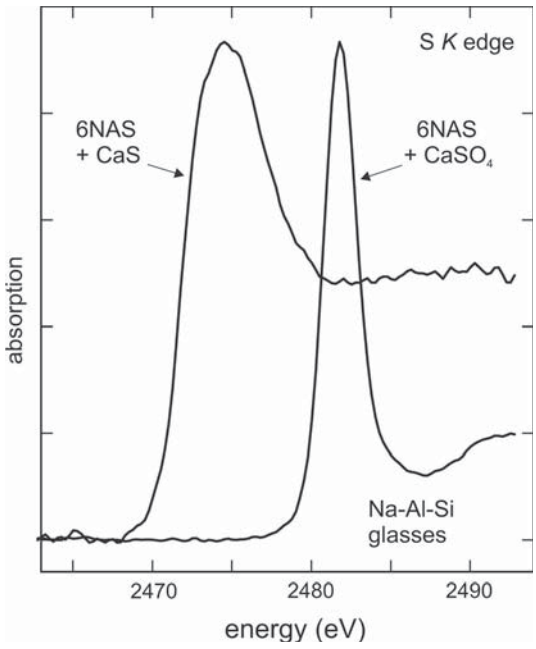

FIG. 16. Sulfur *K*-edge XANES spectra for quenched Na–Ca-aluminosilicate melts, showing a pronounced shift in absorption-edge peak from monosulfide (2– oxidation state; added as CaS) to sulfate (6+; added as $CaSO_4$); NAS is $NaAlSiO_4$ (after Fleet *et al*. 2005a).

The S *K*-edge XANES spectra of basaltic glasses synthesized under reducing conditions (*i.e*., close to the wüstite–magnetite and iron – quartz – fayalite oxygen buffers) are dominated by a single broad absorption peak extending from 2470 to 2482 eV, in combination with a weak peak or shoulder at 2470–2471 eV, and can be reproduced by mixing XANES spectra for FeS and alkaline-earth monosulfides (Fig. 17). The weak peak at 2470–2471 eV corresponds to the photoelectron transition S $1s \rightarrow$ [S $3p$ σ*, Fe $3d(e_g)$] in NiAs-type (B8) FeS (peak **a** in Fig. 6), and represents Fe monosulfide dissolved in glasses (and melts): it is diminished and shifted in energy relative to the spectrum for $Fe_{0.923}S$ because the stereochemical environment of S^{2-} is different in the glass than in the Fe sulfide. The first co-ordination sphere of sulfide atoms in basaltic glass probably also contains a small proportion of alkaline-earth and alkali cations, particularly Ca^{2+}. This is not too surprising, as the molar content of CaO makes a significant contribution to the S capacity of laboratory-equilibrated basaltic melts (Haughton *et al*. 1974, O'Neill & Mavrogenes 2002). In agreement with this expectation, the S *K*-edge XANES of the glass PG35 can be reproduced by mixing the spectra for troilite (FeS) and niningerite (MgS) in the ratio 3:2, and that of 1652–4 by mixing these sulfide spectra in the ratio 4:1: the XANES spectrum for MgS is used here as a proxy for CaS "dissolved in the glass". The S *K*-edge XANES spectra for basalts from the eastern Galapagos rift display a wider variation in features than the synthetic

basaltic glasses (Fig. 17), no doubt reflecting more varied redox conditions and quenching and cooling histories. However, these spectra are also dominated by sulfide, and one spectrum (for sample 1652–5) shows trace sulfate.

Lazurite and Haüyne

XANES spectroscopy has been used to study the chemical state of S in phosphate and silicate minerals. Minor amounts of S in apatite are present as sulfate (Paris *et al.* 2001) substituting for the phosphate group. Fleet *et al.* (2005b) recently investigated the sodalite-group minerals lazurite (Hogarth & Griffin 1976) and haüyne (Taylor 1967), which accommodate various S species within the interstices of an aluminosilicate framework,

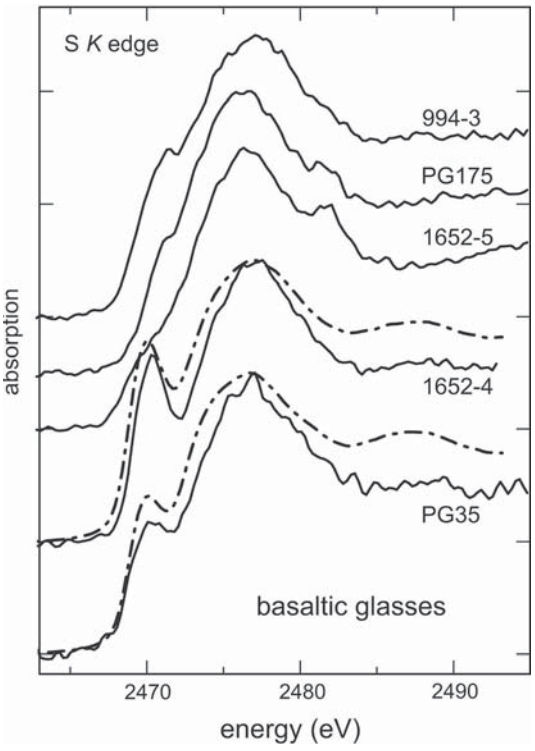

Fig. 17. Sulfur *K*-edge XANES spectra for basaltic glasses synthesized under reducing conditions (PG175 and PG35) and collected from the eastern Galapagos rift (994–3, 1652–5 and 1652–4). The S contents (wt.%) are 0.08(1) and 0.10 for PG35, 0.11(1) and 0.12 for 994–3, 0.10(1) and 0.09 for 1652–5 and 0.11(1) and 0.10 for 1652–4 using EPMA and XANES area, respectively, with the latter method calibrated against PG175 with 0.15(2) wt.% S by EPMA. Note that XANES spectra for 1652–4 and PG35 are simulated by mixing XANES for FeS and MgS (proxy for CaS) in ratios of 4:1 and 3:2, respectively (after Fleet *et al.* 2005a).

and made some preliminary observations on scapolite. The cage anions in lazurite [$Na_6Ca_2Al_6Si_6O_{24}(SO_4,S)_2$] are predominantly reduced species of S and sulfate, and the mineral is notable for its color (rich royal blue, azure, violet-purple, and greenish blue), being prized as a blue pigment from antiquity. In contrast, S is completely oxidized in haüyne [$Na_6Ca_2Al_6Si_6O_{24}(SO_4)_2$], and the mineral is colorless in the pure form. Crystal-chemical interest in these minerals is piqued by developments in the chemical composition of ultramarine pigments, which are sodalite-group phases with assumed formulae of $Na_8Al_6Si_6O_{24}S_4$, $Na_{6.9}Al_{5.6}Si_{6.4}O_{24}S_{2.0}$, $Na_6Al_6Si_6O_{24}{\bullet}NaS_3$, *etc.* (*e.g.*, Clark *et al.* 1983, Gobeltz *et al.* 1998, Reinen & Lindner 1999, Gobeltz-Hautecoeur *et al.* 2002). It is generally accepted in these studies that the characteristic color of ultramarine pigments is associated with their reduced S content and, specifically, with the presence of polysulfide S_3^- and S_2^- radical anion color-centers. The polysulfide radical S_3^- is thought to be the dominant chromophore in royal-blue lazurite and blue ultramarine pigments.

Lazurite was synthesized in Fleet *et al.* (2005b) using (CaS + $CaSO_4$) auto-redox in hydrothermal experiments and reduction with Re foil in piston–cylinder experiments. The S *K*-edge XANES spectra for selected experimental products and royal-blue lazurite from Afghanistan (No. 2746) and Baffin Island (No. 1343) are compared in Figure 18. The spectrum of synthetic haüyne (experiment LZ11) has a single sharp edge-peak at 2481.7 eV, consistent with sulfate bonded to Ca and Na. The spectrum of a royal-blue lazurite (experiment LZ67), formed by annealing at 1200°C and 0.5 GPa, is dominated by sulfate (edge peak at 2481.7 eV) with minor reduced S species (edge peak at 2471.0 eV); on the basis of fitted peak-areas, reduced S amounts to only about 4.4% of total S. The sulfate component of this XANES spectrum is in excellent agreement with the S *K*-edge XANES spectrum of LZ11 (Fig. 18), indicating that sulfate is bonded to both Ca and Na, but the reduced S species is bonded only to Na (note that S^{2-} bonded to Ca would result in an edge peak near 2475 eV). The S *K*-edge XANES spectra for royal-blue lazurite from Afghanistan and Baffin Island are also dominated by the sulfate edge, with subordinate reduced S amounting to 15 and 11% of total S, respectively (Fig. 18): the spectrum for the Baffin Island lazurite essentially duplicates an earlier measurement by Cade (2003). However, the S *K*-edge XANES spectra do not provide an unambiguous test for the presence of the putative chromophore responsible for the royal-blue color of lazurite (the polysulfide species S_3^-), because the absorption edges for disulfide, other polysulfides and sulfide bonded to alkali and alkaline earth cations all crowd into the spectral range from 2471 to 2475 eV. Fortunately, complementary X-ray photoelectron spectroscopy (XPS) showed that the reduced S in these materials is almost exclusively sulfide, and that polysulfides are not present above minimum levels of detection (Fleet *et al.*

2005b). Note that the S *K*-edge XANES spectra for blue lazurite from hydrothermal experiments showed that the reduced S component in the framework cages is mainly thiosulfate (*cf*. experiment LZ07 in Fig. 18 and sodium thiosulfate in Fig. 14).

Organic Geochemistry

Chemical groups containing nitrogen and S comprise a significant fraction of the functional sites on humic substances and play major roles in interacting with inorganic and organic contaminants (*e.g*., Vairavamurthy *et al*. 1997). The soil environment is the primary component of the global biogeochemical S cycle, acting as both a source and sink for various S species and mediating changes in oxidation states. The organic geochemistry of S is complex, and natural organic matter typically contains both reduced and oxidized S species. The reduced S species occur largely as intramolecular bridges (*e.g*., sulfide C–S–C, disulfide C–S–S–C and polysulfide C–S–S_n–S–C bridges) in the high-molecular-weight cross-linked heterogeneous organic material. The sulfide bridge H_2C–S–S–CH_2 in cystine ($C_6H_{12}N_2O_4S_2$) is a fairly simple example, and cross-linking disulfide bridges (C–S–S–C) are important in stabilizing the structures of protein molecules. On the other hand, the oxidized forms of S (*i.e*., sulfonates and ester-bonded sulfates) are present only as terminal groups of the organic molecules in question. Vairavamurthy *et al*. (1997) noted that although the reduced S and sulfonate species may be formed by both biochemical and geochemical pathways, there is no known geochemical route for forming ester-bonded sulfates. Almost all of the organic S in soils and riverine systems is of biological origin. In contrast, the dominant fraction of the organic S in marine sediments is considered to be of diagenetic origin, and a product of the reaction of S nucleophiles with functionalized organic molecules coating clay minerals. Active S nucleophiles include the hydrogen sulfide generated in bacterial sulfate reduction and its partial oxidation intermediates, such as thiols and polysulfides. Thus, when a thiol group is added across an unsaturated bond of a functional organic site, an organic S bond (*i.e*., C–S–) is formed, nucleating a bridging organic reaction. Sulfur nucleophiles also react with Fe-bearing minerals, in the inorganic branch of the S cycle, to form Fe sulfides, principally pyrite and pyrrhotite.

The chemical complexity of natural organic matter has frustrated its routine biogeochemical characterization. In soil science, reduction with hydrogen iodide (HI) is a standard procedure for distinguishing between ester–SO_4–S (HI-reducible S) and C-bonded S. However, this indirect method yields only limited biochemical characterization of organic S (*e.g*., Solomon *et al*. 2003). Differential reduction of organic S compounds to H_2S does not identify the organic functional groups or the intermediate oxidation states of S. The pyrolysis – gas chromatography – mass spectrometry approach is used for coal, kerogens and aquatic humic substances, but is limited to speciation of thermally stable forms of S. Within this context, S *K*- and *L*-edge XANES spectroscopy are proving to be invaluable, non-destructive, and in some cases *in situ*, techniques for characterizing the S functional groups in natural organic matter. The method has been applied to coals (*e.g*., Hussain *et al*. 1982, Spiro *et al*. 1984, Huffman *et al*. 1991, 1995, George *et al*. 1991, Brown *et al*. 1992, Kasrai *et al*. 1990, 1996b, Olivella *et al*. 2002, Huggins *et al*. 1997), heavy petroleum asphalts (bitumens) and asphaltenes (George & Gorbaty 1989, Gorbaty *et al*. 1991, Waldo *et al*. 1991, Kasrai *et al*. 1994, Vairavamurthy *et al*. 1994, Sarret *et al*. 1999), kerogens (Eglinton *et al*. 1994, Sarret *et al*. 2002) and sediments, soils and humus (Vairavamurthy *et al*. 1994, 1997, Morra *et al*. 1997, Olivella *et al*. 2002, Qian *et al*. 2002, Beauchemin *et al*. 2002, Solomon *et al*. 2003, Jokic *et al*. 2003).

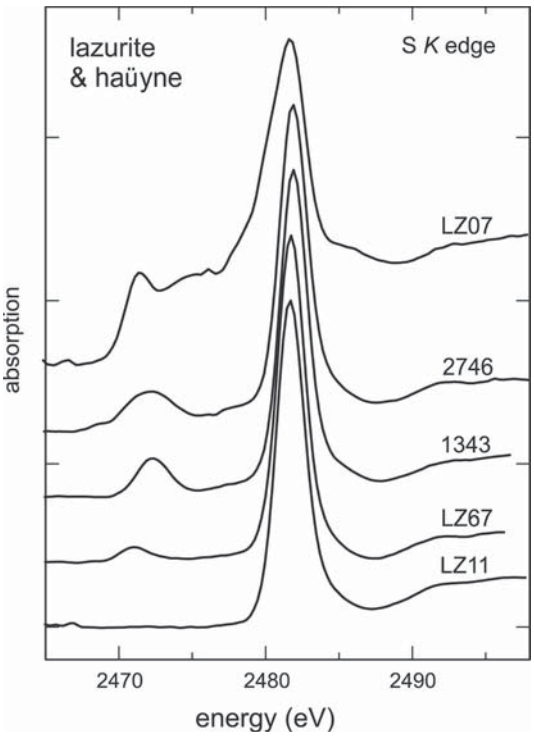

FIG. 18. Sulfur *K*-edge XANES spectra for synthetic haüyne (LZ11) and lazurite from Afghanistan (2746), Baffin Island (1343) and high- (LZ67) and hydrothermal-pressure (LZ07) synthesis. Note that the spectrum of colorless haüyne contains a single edge-peak for sulfate, whereas royal-blue lazurite (2746, 1343 and LZ67) contains both reduced S and sulfate species, and LZ07 contains thiosulfate and sulfate species (after Fleet *et al*. 2005b).

Sulfur is one of the major and most troublesome contaminants in fossil fuels. Although it is present only in low concentrations, S causes problems in every process that involves coal. Both the content and chemical form of S vary considerably with provenance and rank of the coal. The presence of organically bound S, which cannot be removed by physical coal-cleaning methods, is a major obstacle in the use of high-S coals: the inorganic-S content, which is principally in the form of pyrite and sulfate minerals, is readily removed by physical methods (*e.g.*, Huggins *et al.* 1997). The potential applications of S *K*-edge XANES spectroscopy for fingerprinting and quantifying S in coal was explored by Hussain *et al.* (1982), who showed that the absorption at the S *K* edge is qualitatively in proportion to the amount of S present in lignite (1.1 wt.% S), semanthracite (0.6 wt.% S), subbituminous coal (0.4 wt. % S) and a bituminous (high volatile content) coal (3.6 wt.% S). The S *K*-edge XANES method was used to characterize and quantify organic S species in a number of subsequent studies (George & Gorbaty 1989, George *et al.* 1991, Huffman *et al.* 1991, Huggins *et al.* 1997). The different functional S groups were resolved by least-squares fitting by Huffman *et al.* (1991) and third-derivative analysis by George *et al.* (1991). Kasrai *et al.* (1990, 1996b) and Brown *et al.* (1992) developed S *L*-edge XANES spectra for fingerprinting the functional groups of organic S in coals. In the most recent of these three studies, linear combinations of the S *L*-edge XANES spectra for various inorganic and organic model compounds (Figs. 3, 19) were used for reference purposes. Kasrai *et al.* (1996b) characterized Rasa coal (a bituminous coal from Croatia of Cretaceous age), P–803 coal (bituminous, Canada, Cretaceous) and fossilized latex-1 and -2 (Germany, Eocene), identifying alkyl and aryl sulfides, alkyl and aryl disulfides and heterocyclic forms of sulfur in powdered samples of the untreated coals. Sulfonic acid and sulfate were present in coal oxidized in air. For the untreated Rasa coal, in which S is mostly of organic origin, they found that the best match of the S *L*-edge XANES spectrum (Fig. 19) was obtained with a composite spectrum modeled from 40% of the spectrum of 1,2-benzodiphenylene sulfide (thiophenic S), 30% thioxanthen-9-one and 30% phenyl (aryl) disulfide (spectra B, C and D, respectively, in Fig. 19), in good agreement with the earlier estimate of Brown *et al.* (1992). In respect to the appropriate X-ray absorption methodology for characterizing organic S in coals, Kasrai *et al.* (1996b) concluded that whereas both S *K*- and *L*-edge XANES spectra are sensitive to S functional groups, the S *L*-edge method is more sensitive to subtle changes in the substitutions within individual functional groups.

Sulfur speciation in kerogens of the Orbagnoux deposit (southern Jura Mountains, France; Upper Kimmeridgian in age) have been studied by S *K*- and *L*-edge XANES spectroscopy and pyrolysis (Sarret *et al.* 2002). The deposit is noted for conspicuous accumulations of oil-bearing, thermally immature, and extremely S-rich organic matter: S contents as high as 17.5 wt.% have been reported for some samples of isolated kerogens. The kerogens were concentrated from rock powders by solvent extraction and acid treatment, and investigated in powdered form. The S *L*-edge XANES spectra of the unheated kerogens are characterized by three main peaks (labeled **a**, **b** and **c** in Fig. 20) that correspond in energy position to the principal features

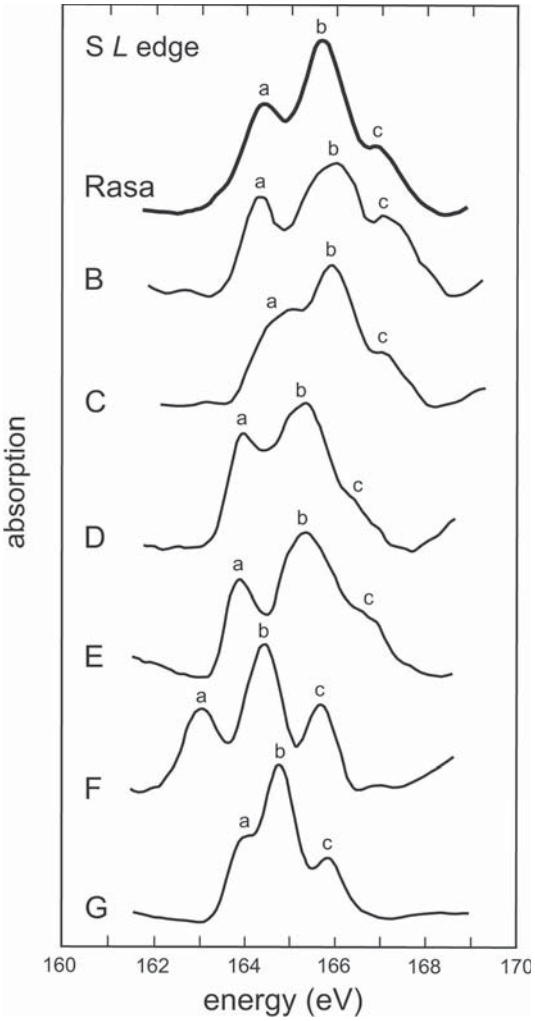

FIG. 19. Sulfur *L*-edge XANES spectra for a standard coal from Rasa (Croatia) and reference organic S compounds, including: (B) 1,2-benzodiphenylene sulfide, (C) thioxanthen-9-one, (D) phenyl disulfide, (E) poly(phenylene sulfide), (F) DL-cystine and (G) S-methyl-L-cysteine. The best match for the Rasa coal was obtained with 40% thiophenic S (B), 30% thioxanthone (C) and 30% aryl disulfide (D) (after Kasrai *et al.* 1996b).

in the XANES spectrum of thiophene (spectrum E in Fig. 20). Satisfactory matches to both S *K*- and *L*-edge XANES spectra of kerogens were obtained with linear combinations of the spectra for the labeled compounds; *e.g.*, the S *L*-edge XANES for sample TM9sa was modeled with 66% thiophene, 22% thiol S and 12% disulfide (spectra E, B and A, respectively, in Fig. 20). Sarret *et al*. (2002) showed that S speciation is similar in the unheated kerogens from the five facies recognized in the Orbagnoux deposit; all samples examined contain thiophenes as major species and disulfides, alkyl sulfide and thiols in smaller proportion. Also, substantial aromatization of non-thiophenic S forms occurred with thermal treatment.

Sulfur *K*-edge XANES spectroscopy has been used to identify oxidation states of S and assess the impact of land-use changes on organic S in soils from two localities in Ethiopia (Solomon *et al*. 2003). XANES spectra for humic substances extracted from the clay-size fraction of soils from the southwestern highlands at Wushwush are shown in Figure 21, where the energy scale is relative to the edge feature of native S at 2472 eV. Reduced S species are characterized by absorption at 0.8–1.8 eV (representing sulfide, disulfide, thiol and thiophene), intermediate species at 1.9–2.5 eV (sulfoxide) and 8.2–8.5 eV (sulfonate), and oxidized species at 10.1–10.2 eV (sulfate). Evidently, the intermediate oxidation-states (sulfoxide and sulfonate) are dominant in organic matter associated with the clay-size fraction, followed by highly oxidized S and most reduced S. The relative proportion of most reduced and intermediate S species decreased overall in the sequence natural forests > plantations > cultivated fields. The S XANES are critical to understanding the link between S oxidation states, bioavailability of organic S moieties and the shifts that occur following land-use changes.

Sulfur *K*-edge XANES spectra of marine sediments and extracted humic substances from three diverse localities (a salt marsh in Shelter Island, New York, the Peru Margin and Florida Bay) show that organic sulfides, disulfides and polysulfides, sulfonates and organic sulfates are the major forms of S (Fig. 22; Vairavamurthy *et al*. 1997). The bulk-sediment samples from the salt marsh and Peru Margin also contain significant amounts of pyrite. The absence of pyrite from the Florida Bay sediment was attributed to the very low Fe content of the carbonate sediments, although it seems clear from the decrease in proportion of total reduced S content that the redox conditions are more oxidizing in the sequence salt marsh < Peru Margin < Florida Bay. As noted above, although the reduced and intermediate-oxidation-state S species in humic substances may be formed by both biochemical and geochemical processes, there is no known geochemical route for forming ester-bonded sulfates. Thus, in marine sediments, these terminal groups are either inherited from the source organic matter or formed by bacterial mediation. Contrary to an earlier view that it is unstable

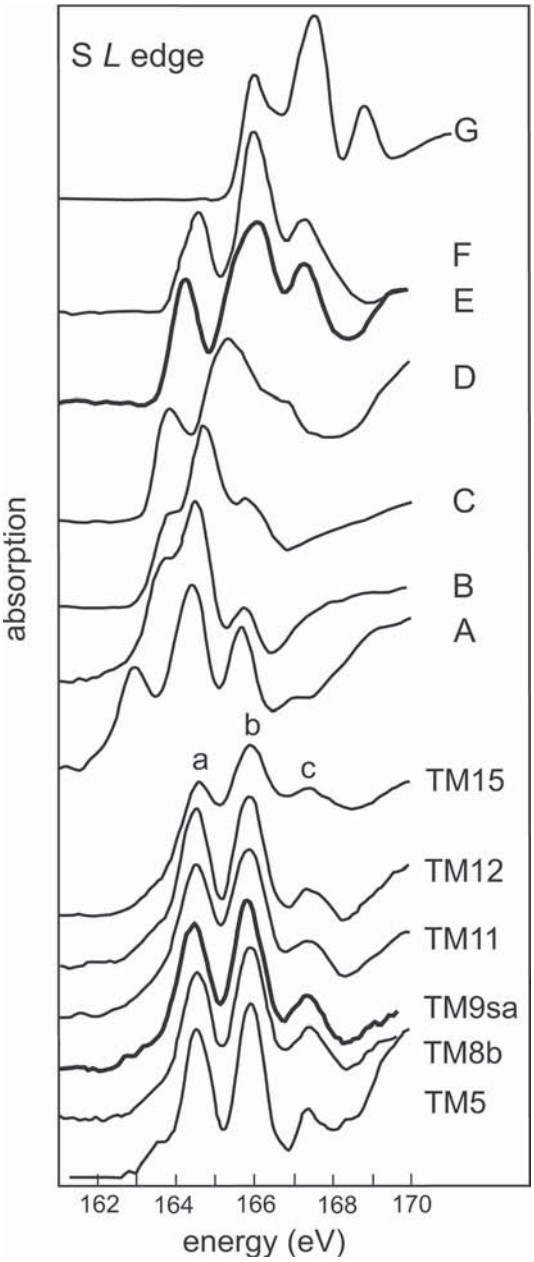

FIG. 20. Comparison of S *L*-edge XANES spectra for kerogens from Orbagnoux (France; TM5, TM8b, TM9sa, TM11, TM12 and TM15) and some reference organic S compounds, including: (A) DL-cystine, (B) DL-cysteine, (C) DL-methionine, (D) poly(phenylene sulfide), (E) dibenzothiophene, (F) 3-(2-thienyl)-DL-alanine and (G) DL-methionine sulfoxide. The best match for kerogen sample TM9sa was obtained with 66% thiophene (E), 22% thiol S (B) and 12% disulfide (A) (after Sarret *et al*. 2002).

in marine sediments, Vairavamurthy *et al*. (1997) showed that ester-bonded sulfate is a major form of S in sedimentary humic substances and can survive the exhaustive pH changes involved in extracting humic acids from sediments. Recognition of the cross-linking structural role of the reduced S species shows that the organic C–S–C linkages are generated during humification in the early stages of diagenesis, thus supporting the argument that humic substances are the precursors of source-rock kerogens.

In other related S *K*-edge XANES studies, Jokic *et al*. (2003) analyzed S speciation in wetland soils from Saskatchewan, and Qian *et al*. (2002) found that methyl mercury, $CH_3Hg(II)$, preferentially forms complexes with reduced organic S groups of humic substances in northern soils and stream sediments. With the advent of high-brightness synchrotron-radiation beams, spatial mapping of S species is now possible. Thus, S *K*-edge XANES mapping allows the location of the sulfated glucidic components of coral aragonite skeletons to be identified (Cuif *et al*. 2003). In that study, the authors used the two amino acids cysteine (H–S–C bonds) and methionine (C–S–C bonds) as well as cystine (C–S–S–C bonds) as reference compounds for reduced S, and chondroitin sulfate ($C–SO_4$ bonds), a sulfated sugar, for oxidized S. The XANES mapping showed that high concentrations of sulfated sugars coincide with centers of calcification, with lesser amounts of sulfated sugars located at skeletal growth steps, strongly suggesting involvement of sugars in the mineralization process.

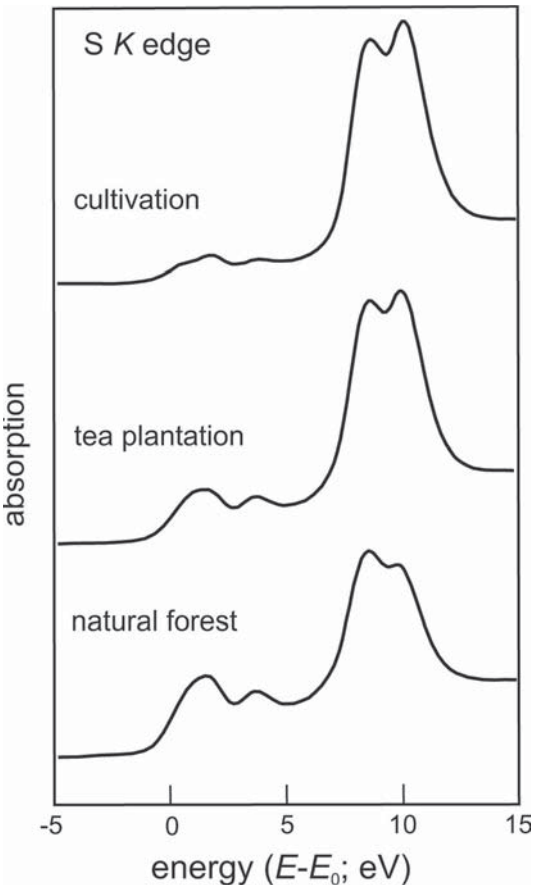

FIG. 21. Sulfur *K*-edge XANES spectra for humic substances extracted from clay (<2 μm) separates of soils from Wushwush, southwestern highlands of Ethiopia, showing progressive loss of reduced and intermediate-oxidation-state S with more extensive cultivation. The photoelectron energy is relative to the absorption threshold (after Solomon *et al*. 2003).

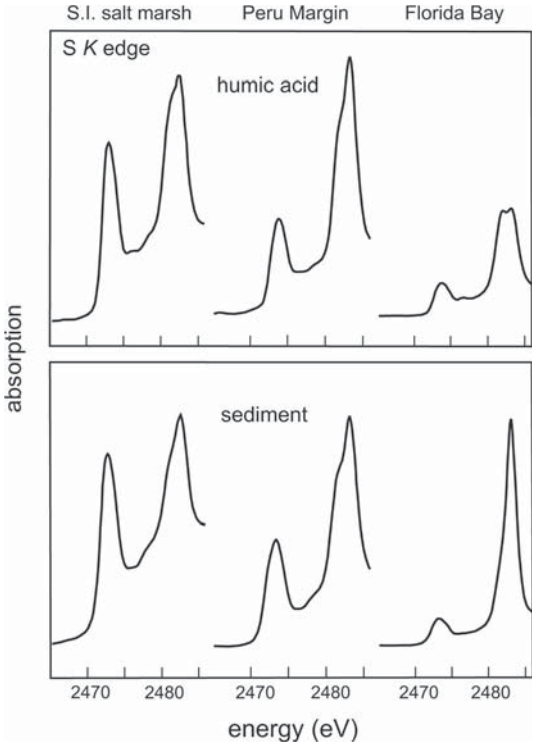

FIG. 22. Sulfur *K*-edge XANES spectra for humic-acid extracts from near-surface (6–14 cm depth) sediment and corresponding whole sediment, from the Shelter Island, New York, salt marsh, Peru Margin and Florida Bay, showing significant proportions of reduced, intermediate-oxidation-state and oxidized organic S (edge peaks at 2473, 2474–2481 and 2483 eV, respectively; after Vairavamurthy *et al*. 1997).

Summary

(1) The fine structure at X-ray absorption edges has given rise to two quite different types of chemical spectroscopy: extended X-ray absorption fine structure (EXAFS) and X-ray absorption near-edge structure (XANES). The XANES spectrum is a fingerprint of the chemical state of the absorber atom, and XANES spectroscopy has proven to be the ideal non-destructive technique for characterizing and quantifying S species in compositionally complex natural materials.

(2) The S *K* edge corresponds to transition of photoelectrons from the S 1*s* core level to unoccupied S 3*p* σ* antibonding orbitals, and the S *L* edge to transition from the S 2*p* core level to empty S 3s σ* antibonding orbitals. The 2*p* level is split by spin–orbit interaction, so that the actual photoelectron transitions for the latter are S $2p_{3/2} \rightarrow$ S 3*s* σ* and S $2p_{1/2} \rightarrow$ S 3*s* σ*. Because both initial and final electron states are important in defining the transition energy associated with an absorption edge, the XANES spectrum yields information on the lower part of the conduction band, and the chemical state and local stereochemical environment of the S absorber atom. Moreover, through hybridization of unoccupied S antibonding orbitals and empty metal 3*d* orbitals, S *K*- and *L*-edge XANES spectra also reveal details of the 3*d* electron configuration and bonding of metal atoms coordinated with S, even though the metal atoms are not probed directly.

(3) The position of the edge feature of S *K*- and *L*-edge XANES is a chemical ruler for oxidation states of S. The S *K* edge shifts progressively from 2469.5–2470 eV for transition-metal monosulfides (2– oxidation state) to 2471 eV for disulfides of the pyrite group (1–), 2472 eV for native S (0), 2478 eV for sulfites (4+) and 2482 eV for sulfates (6+). The complex S oxyanions may exhibit a characteristic edge for each functional S group and even for individual S–S and S–O bonds. Similar shifts are evident for organic S: *e.g.*, in humic substances from soils in Ethiopia, reduced S species are characterized by absorption at 2473–2474 eV (representing sulfide, disulfide, thiol and thiophene), intermediate species at 2474–2475 eV (sulfoxide) and 2480–2481 eV (sulfonate) and oxidized species at 2482 eV (sulfate). A complicating factor for inorganic calibration is that the S *K* edge of monosulfides also shifts upward with decreasing covalence of the metal, from 2469.5 eV in chalcopyrite to 2475.1 eV in niningerite.

(4) Sulfur *K*-edge XANES spectra are reviewed for chalcopyrite, arsenopyrite, pyrite, troilite, pyrrhotite and NiAs-type $Co_{0.923}$ and $Ni_{0.923}S$, niningerite (MgS), oldhamite (CaS), alabandite (MnS) and cubic FeS, sphalerite and related phases and selected solid-solutions of the monosulfides. The XANES spectra for FeS, CoS, NiS, MgS, CaS, MnS and ZnS have been simulated by multiple-scattering calculations. A common characteristic feature of the S *K*-edge XANES is that the strength of the edge peak of the NiAs-type monosulfides, and their mutual solid-solutions, and of a shoulder to the edge peak of the cubic monosulfide and sphalerite- or wurtzite-type solid-solutions, increases progressively with increase in participation of metal 3*d* orbitals in metal–S bonding.

(5) The edge features of S *L*-edge XANES spectra for the ferrous-metal monosulfides tend to be diffuse and weakly developed above background. However, complexity in the S L_2,L_3 edges of troilite, pyrrhotite and CdI_2-type TiS_2 is consistent with crystal-field splitting of the final state S3s σ* antibonding orbitals hybridized with empty Fe 3*d* orbitals.

(6) Sulfate in gypsum, anhydrite, celestine, barite and other inorganic salts, silicate minerals and glasses and organic compounds is characterized by a single sharp *K*-edge feature at 2482 eV.

(7) The S *K*-edge XANES spectra of reduced basaltic glasses are dominated by a single broad absorption peak extending from 2470 to 2482 eV in combination with a weak peak or shoulder at 2470–2471 eV, and can be reproduced by mixing XANES spectra for FeS and alkaline-earth monosulfides. Thus, the first coordination sphere of sulfide atoms in basaltic glasses probably also contains a small proportion of Ca^{2+}, in addition to Fe cations. More oxidized silicate glasses contain sulfate coexisting with sulfide.

(8) The S *K*-edge XANES spectra of royal-blue lazurite are dominated by the sulfate edge, with subordinate reduced S species amounting to 15 and 11% of total S for samples from Afghanistan and Baffin Island, respectively, and 4.4% for a synthetic sample annealed at 1200°C and 0.5 GPa. However, the XANES method did not provide an unambiguous test for the presence of the polysulfide (S_3^-) chromophore.

(9) Sulfur *K*- and *L*-edge XANES spectroscopy are proving to be invaluable non-destructive, and in some cases *in situ*, techniques for characterizing and quantifying the sulfur functional groups in natural organic matter. For example, S *L*-edge XANES spectra were used to identify alkyl and aryl sulfides, alkyl and aryl disulfides and heterocyclic forms of sulfur in untreated coals and sulfonic acid and sulfate in coal oxidized in air. Similarly, by using linear combinations of reference spectra, kerogen from the Orbagnoux deposit, France, was deduced to contain 66% thiophene, 22% thiol sulfur and 12% disulfide species. Sulfur *K*-edge XANES shows that the major forms of organic S in humic substances extracted from marine sediments are sulfides, disulfides and polysulfides, sulfonates and sulfates. Also, the proportion of reduced organic S species diminishes with cultivation in subtropical soils. The recent introduction of S *K*-edge micro-XANES mapping has shown that sulfated sugars are concentrated at the centers of calcification of coral aragonite skeletons, suggesting an involvement of the sugars in the mineralization process.

Acknowledgements

I thank F.C. Hawthorne and G.S. Henderson for helpful comments, staff of the Canadian Synchrotron Radiation Facility and Synchrotron Radiation Centre (SRC), University of Wisconsin – Madison, for their technical assistance, and the National Science Foundation (NSF) for support of the SRC. This work was supported by the Natural Sciences and Engineering Research Council of Canada.

References

Ankudinov, A.L., Ravel, B., Rehr, J.J. & Conradson, S.D. (1998): Real space multiple-scattering calculation and interpretation of x-ray-absorption near-edge structure. *Phys. Rev. B* **58**, 7565-7576.

Bancroft, G.M. (1992): New developments in far UV, soft X-ray research at the Canadian Synchrotron Radiation Facility. *Can. Chem. News* **44**, 15-22.

Beauchemin, S., Hesterberg, D. & Beauchemin, M. (2002): Principal component analysis approach for modeling sulfur K-XANES spectra of humic acids. *Soil Sci. Soc. Am. J.* **66**, 83-91.

Bianconi, A. (1988) XANES Spectroscopy. *In* X-ray Absorption: Principles, Applications and Techniques of EXAFS, SEXAFS and XANES. Chemical Analysis, Vol. **92** (D.C. Koningsberger & R. Prins, eds.). John Wiley & Sons, New York, N.Y. (573-662).

Bocharov, S., Dräger, G., Heumann, D., Šimůnek, A. & Šipr, O. (1998): Polarized x-ray-absorption spectra of TiS_2, $TiSe_2$, and $TiTe_2$. *Phys. Rev. B* **58**, 7668-7674.

Bonnin-Mosbah, M., Métrich, N., Susini, J., Salomé, M., Massare, D. & Menez, B. (2002): Micro X-ray absorption near edge structure at the sulfur and iron *K*-edges in natural silicate glasses. *Spectrochim. Acta B* **57**, 711-725.

Brown, J.R., Kasrai, M., Bancroft, G.M., Tan, K.H. & Chen, J.M. (1992): Direct identification of organic sulfur species in Rasa coal from sulfur L-edge X-ray absorption near edge spectra. *Fuel* **71**, 649-653.

Bunker, G. & Stern E.A. (1984): Experimental study of multiple scattering in X-ray-absorption near-edge structure. *Phys. Rev. Lett.* **52**, 1990-1993.

Cade, A.M. (2003): *Colouration of Lazurite from Baffin Island, Nunavut*. M.Sc. thesis, University of Western Ontario, London, Ontario.

Chen, J.G. (1997): NEXAFS investigations of transition metal oxides, nitrides, carbides, sulfides and interstitial compounds. *Surf. Sci. Rep.* **30**, 1-152.

Clark, R.J.H., Dines, T.J. & Kurmoo, M. (1983): On the nature of the sulphur chromophores in ultramarine blue, green, violet, and pink and of the selenium chromophore in ultramarine selenium: characterization of radical anions by electronic and resonance Raman spectroscopy and the determination of their excited-state geometries. *Inorg. Chem.* **22**, 2766-2772.

Cuif, J.-P., Dauphin, Y., Doucet, J., Salomé, M. & Susini, J. (2003): XANES mapping of organic sulfate in three scleractinian coral skeletons. *Geochim. Cosmochim. Acta* **67**, 75-83.

Della Longa, S., Soldatov, A., Pompa, M. & Bianconi, A. (1995): Atomic and electronic structure probed by X-ray absorption spectroscopy: full multiple scattering analysis with the G4XANES package. *Comput. Mater. Sci.* **4**, 199-210.

Dijkstra, J., van Bruggen, C.F., Haas, C. & de Groot, R.A. (1989): Electronic band-structure calculations of some magnetic chromium compounds. *J. Phys.: Condensed Matter* **1**, 9163-9174.

Durham, P.J. (1988): Theory of XANES. *In* X-ray Absorption: Principles, Applications and Techniques of EXAFS, SEXAFS and XANES. Chemical Analysis, Vol. **92** (D.C. Koningsberger & R. Prins, eds.). John Wiley & Sons, New York, N.Y. (53-84).

Eglinton, T.I., Irvine, J.E., Vairavamurthy, A., Zhou, W. & Manowitz, B. (1994): Formation and diagenesis of macromolecular organic sulfur in Peru margin sediments. *Organic Geochem.* **22**, 781-799.

Farrell, S.P. & Fleet, M.E. (2000): Evolution of local electronic structure in cubic $Mg_{1-x}Fe_xS$ by S *K*-edge XANES spectroscopy. *Solid State Commun.* **113**, 69-72.

_____ & _____ (2001): Sulfur K-edge XANES study of local electronic structure in ternary monosulfide solid solution [$(Fe, Co, Ni)_{0.923}S$]. *Phys. Chem. Minerals* **28**, 17-27.

_____, _____, Stekhin, I.E., Kravtsova, A., Soldatov, A.V. & Liu, Xiaoyang (2002): Evolution of local electronic structure in alabandite and niningerite solid solutions [(Mn,Fe)S, (Mg,Mn)S, (Mg,Fe)S] using sulfur *K*- and *L*-edge XANES spectroscopy. *Am. Mineral.* **87**, 1321-1332.

Fleet, M.E., Harmer, S.L., Liu, Xiaoyang & Nesbitt, H.W. (2005c): Polarized X-ray absorption spectroscopy and XPS of TiS_3: S *K*- and Ti *L*-edge XANES and S and Ti 2*p* XPS. *Surface Science* **584**, 133-145.

_____ & Liu, Xiaoyang (2001): Boron K-edge XANES of boron oxides: tetrahedral B–O distances and near-surface reconstruction. *Phys. Chem. Minerals* **28**, 421-427.

_____, _____, Harmer, S.L. & King, P.L. (2005a): Sulfur K-edge XANES spectroscopy: chemical state and content of sulfur in silicate glasses. *Can. Mineral.* **43**, 1605-1618.

_____, _____, _____ & Nesbitt, H.W. (2005b): Chemical state of sulphur in natural and synthetic lazurite

by S *K*-edge XANES and X-ray photoelectron spectroscopy. *Can. Mineral.* **43**, 1589-1603.

_____ & MACRAE, N.D. (1987): Sulfidation of Mg-rich olivine and the stability of niningerite in enstatite chondrites. *Geochim. Cosmochim. Acta* **51**, 1511-1521.

_____ & MUTHUPARI, S. (2000): Boron *K*-edge XANES of borate and borosilicate minerals. *Am. Mineral.* **85**, 1009-1021.

_____, _____, KASRAI, M. & PRABAKAR, S. (1997): Sixfold coordinated Si in alkali and alkali–CaO silicophosphate glasses by Si K-edge XANES spectroscopy. *J. Non-Crystalline Solids* **220**, 85-92.

FUGGLE, J.C. & INGLESFIELD, J.E., eds. (1992): *Unoccupied Electronic States: Fundamentals for XANES, EELS, IPS and BIS*. Topics in Applied Physics **69**. Springer-Verlag, New York, N.Y.

GEORGE, G.N. & GORBATY, M.L. (1989): Sulfur *K*-edge x-ray absorption spectroscopy of petroleum asphaltenes and model compounds. *J. Am. Chem. Soc.* **111**, 3182-3186.

_____, _____, KELEMEN, S.R. & SANSONE, M. (1991): Direct determination and quantification of sulfur forms in coals from the Argonne premium sample program. *Energy Fuels* **5**, 93-97.

GOBELTZ, N., DEMORTIER, A., LELIEUR, J.P. & DUHAYON, C. (1998): Correlation between EPR, Raman and colorimetric characteristics of the blue ultramarine pigments. *J. Chem. Soc., Faraday Trans.* **94**, 677-681.

GOBELTZ-HAUTECOEUR, N., DEMORTIER, A., LEDE, B., LELIEUR, J.P. & DUHAYON, C. (2002): Occupancy of the sodalite cages in the blue ultramarine pigments. *Inorg. Chem.* **41**, 2848-2854.

GOODENOUGH, J.B. (1967): Description of transition metal compounds: application to several sulfides. *In* Propriétés Thermodynamiques Physiques et Structurales des Dérivés Semi-Métalliques. Centre National de la Recherche Scientifique, Paris, France (263-292).

GORBATY, M.L., GEORGE, G.N. & KELEMEN, S.R. (1991): Direct determination and quantification of sulfur forms in heavy petroleum and coal: sulfur K-edge X-ray absorption and X-ray photoelectron spectroscopic approaches. *Am. Chem. Soc., Symp. Ser.* **461**, 127-136.

HAUGHTON, D.R., ROEDER, P.L. & SKINNER, B.J. (1974): Solubility of sulfur in mafic magmas. *Econ. Geol.* **69**, 451-467.

HITCHCOCK, A.P., BODEUR, S. & TRONC, M. (1987): Sulfur and chlorine K-shell X-ray absorption spectra of SCl_2, S_2Cl_2, $SOCl_2$, and SO_2Cl_2. *Chem. Phys.* **115**, 93-101.

HOBBS, D. & HAFNER, J. (1999): Magnetism and magneto-structural effects in transition-metal sulphides. *J. Phys.: Condensed Matter* **11**, 8197-8222.

HOGARTH, D.D. & GRIFFIN, W.L. (1976): New data on lazurite. *Lithos* **9**, 39-54.

HUFFMAN, G.P., MITRA, S., HUGGINS, F.E., SHAH, N., VAIDYA, S. & LU, F. (1991): Quantitative analysis of all major forms of sulfur in coal by X-ray absorption fine structure spectroscopy. *Energy Fuels* **5**, 574-581.

_____, SHAH, N., HUGGINS, F.E., STOCK, L.M., CHATTERJEE, K., KILBANE, J.J., II, CHOU, M.M. & BUCHANAN, D.H. (1995): Sulfur speciation of desulfurized coals by XANES spectroscopy. *Fuel* **74**, 549-555.

HUGGINS, F.E., SRIKANTAPURA, S., PAREKH, B.K., BLANCHARD, L. & ROBERTSON, J.D. (1997): XANES spectroscopic characterization of selected elements in deep-cleaned fractions of Kentucky No. 9 coal. *Energy Fuels* **11**, 691-701.

HUSSAIN, Z., UMBACH, E., SHIRLEY, D.A., STÖHR, J. & FELDHAUS, J. (1982): Performance and application of a double crystal monochromator in the energy region $800 \le h\nu \le 4500$ eV. *Nucl. Instrum. Methods* **195**, 115-131.

JOKIC, A., CUTLER, J.N., PONOMARENKO, E., VAN DER KAMP, G. & ANDERSON, D.W. (2003): Organic carbon and sulphur compounds in wetland soils: insights on structure and transformation processes using K-edge XANES and NMR spectroscopy. *Geochim. Cosmochim. Acta* **67**, 2585-2597.

KASRAI, M., BANCROFT, G.M., BRUNNER, R.W., JONASSON, R.G., BROWN, J.R., TAN, K.H. & FENG, X. (1994): Sulfur speciation in bitumens and asphaltenes by X-ray absorption fine structure spectroscopy. *Geochim. Cosmochim. Acta* **58**, 2865-2872.

_____, BROWN, J.R., BANCROFT, G.M., TAN, K.H. & CHEN, J.M. (1990): Characterization of sulphur in coal from sulphur L-edge XANES spectra. *Fuel* **69**, 411-414.

_____, _____, _____, YIN, Z. & TAN, K.H. (1996b): Sulphur characterization in coal from X-ray absorption near edge spectroscopy. *Int. J. Coal Geol.* **32**, 107-135.

_____, FLEET, M.E., BANCROFT, G.M., TAN, K.H. & CHEN, J.M. (1991): X-ray-absorption near-edge structure of alkali halides: the interatomic-distance correlation. *Phys. Rev. B* **43**, 1763-1772.

_____, _____, SHAM, T.K., BANCROFT, G.M., TAN, K.H. & BROWN, J.R. (1988): A XANES study of the S L-edge in sulfide minerals: application to interatomic distance determination. *Solid State Commun.* **68**, 507-511.

_____, LENNARD, W.N., BRUNNER, R.W., BANCROFT, G.M., BARDWELL, J.A. & TAN, K.H. (1996a): Sampling depth of total electron and fluorescence measurements in Si L- and K-edge absorption spectroscopy. *Appl. Surface Sci.* **99**, 303-312.

KAWAI, J., ADACHI, H., HAYAKAWA, S., ZHEN, SONG YANG, KOBAYASHI, K., GOHSHI, Y., MAEDA, K. & KITAJIMA, Y. (1994): Depth selective X-ray absorption fine structure spectrometry. *Spectrochim. Acta* **49B**, 739-743.

KITAMURA, M., SUGIURA, C. & MURAMATSU, S. (1988): Multiple-scattering calculation of sulfur K X-ray absorption spectra for FeS, CoS and NiS. *Solid State Commun.* **67**, 313-316.

KRAVTSOVA, A.N., STEKHIN, I.E., SOLDATOV, A.V., LIU, XIAOYANG & FLEET, M.E. (2004): Electronic structure of *M*S (*M* = Ca,Mg,Fe,Mn): X-ray absorption analysis. *Phys. Rev. B* **69**, 134109/1-134109/12.

KUTZLER, F.W., NATOLI, C.R., MISEMER, D.K., DONIACH, S. & HODGSON, K.O. (1980): Use of one-electron theory for the interpretation of near edge structure in *K*-shell x-ray absorption spectra of transition metal complexes. *J. Chem. Phys.* **73**, 3274-3288.

ŁAWNICZAK-JABŁONSKA, K., IWANOWSKI, R.J., GOŁACKI, Z., TRAVERSE, A., PIZZINI, S., FONTAINE, A., WINTER, I. & HORMES, J. (1996): Local electronic structure of ZnS and ZnSe doped by Mn, Fe, Co, and Ni from X-ray-absorption near-edge structure studies. *Phys. Rev. B* **53**, 1119-1128.

LI, DIEN, BANCROFT, G.M. & FLEET, M.E. (1996): B K-edge XANES of crystalline and amorphous inorganic materials. *J. Electron Spectr. & Related Phenomena* **79**, 71-73.

_____, _____, _____ & FENG, XINGHONG (1995c): Silicon K-edge XANES spectra of silicate minerals. *Phys. Chem. Minerals* **22**, 115-122.

_____, _____, _____, _____ & PAN, YUANMING (1995b): Al *K*-edge XANES spectra of aluminosilicate minerals. *Am. Mineral.* **80**, 432-440.

_____, _____, KASRAI, M., FLEET, M.E., FENG, X. & TAN, K. (1995a): S K- and L-edge X-ray absorption spectroscopy of metal sulfides and sulfates: applications in mineralogy and geochemistry. *Can. Mineral.* **33**, 949-960.

_____, _____, _____, _____, _____, _____ & YANG, B.X. (1994b): Sulfur *K*- and *L*-edge XANES and electronic structure of zinc, cadmium and mercury monosulfides: a comparative study. *J. Phys. Chem. Solids* **55**, 535-543.

_____, _____, _____, _____, _____, YANG, B.X. & TAN, K.H. (1994a): S K- and L-edge XANES and electronic structure of some copper sulfide minerals. *Phys. Chem. Minerals* **21**, 317-324.

LYTLE, F.W., SAYERS, D.E. & STERN, E.A. (1975): Extended x-ray-absorption fine-structure technique. II. Experimental practice and selected results. *Phys. Rev. B* **11**, 4825-4835.

MARFUNIN, A.S. (1979): *Physics of Minerals and Inorganic Compounds*. Springer-Verlag, Berlin, Germany.

MCCAMMON, C.A., JACKSON, I., RINGWOOD, A.E. & CASHION, J.D. (1984): The binary systems FeS – MgS and FeS – MnS: Mössbauer spectroscopy of the B1 solid solutions and high-pressure phase equilibria. *Phys. Chem. Minerals* **11**, 182-193.

MÉTRICH, N., BONNIN-MOSBAH, M., SUSINI, J., MENEZ, B. & GALOISY, L. (2002): Presence of sulfite (S^{IV}) in arc magmas: implications for volcanic sulfur emissions. *Geophys. Res. Lett.* **29**, 33/1-33/4.

_____, SUSINI, J., GALOISY, L., CALAS, G., BONNIN-MOSBAH, M. & MENEZ, B. (2003): X-ray microspectroscopy of sulfur in basaltic glass inclusions. Inference on the volcanic sulfur emissions. *J. Phys. IV: Proc.* **104**, 393-398.

MORRA, M.J., FENDORF, S.E. & BROWN, P.D. (1997): Speciation of sulfur in humic and fulvic acids using X-ray absorption near-edge structure (XANES) spectroscopy. *Geochim. Cosmochim. Acta* **61**, 683-688.

NAKAMURA, M., FUJIMORI, A., SACCHI, M., FUGGLE, J.C., MISU, A., MAMORI, T., TAMURA, H., MATOBA, M. & ANZAI, S. (1993): Metal–nonmetal transition in NiS induced by Fe and Co substitution: X-ray-absorption spectroscopic study. *Phys. Rev.* B **48**, 16942-16947.

NATOLI, C.R., MISEMER, D.K., DONIACH, S. & KUTZLER, F.W. (1980): First-principles calculation of x-ray absorption-edge structure in molecular clusters. *Phys. Rev. A* **22**, 1104-1108.

OKUDE, N., NAGOSHI, M., NORO, H., BABA, Y., YAMAMOTO, H. & SASAKI, T.A. (1999): P and S K-edge XANES of transition-metal phosphates and sulfates. *J. Electron Spectr. Related Phenomena* **103**, 607-610.

OLIVELLA, M.A., DEL RIO, J.C., PALACIOS, J., VAIRAVAMURTHY, M.A. & DE LAS HERAS, F.X.C. (2002): Characterization of humic acid from leonardite coal: an integrated study of PY–GC–MS, XPS and XANES techniques. *J. Anal. Appl. Pyrolysis* **63**, 59-68.

O'NEILL, H.S.C. & MAVROGENES, J.A. (2002): The sulfide capacity and the sulfur content at sulfide saturation of silicate melts at 1400°C and 1 bar. *J. Petrol.* **43**, 1049-1087.

PARIS, E., GIULI, G., CARROLL, M.R. & DAVOLI, I. (2001): The valence and speciation of sulfur in glasses by X-ray absorption spectroscopy. *Can. Mineral.* **39**, 331-339.

PERFIT, M.R., FORNARI, D.J., MALAHOFF, A. & EMBLEY, R.W. (1983): Geochemical studies of abyssal lavas recovered by DSRV *Alvin* from eastern Galapagos Rift, Inca transform, and Ecuador Rift. 3. Trace element abundances and petrogenesis. *J. Geophys. Res. B* **88**, 10551-10572.

PONG, W.F., MAYANOVIC, R.A, WU, K.T., TSENG, P.K., BUNKER, B.A., HIRAYA, A. & WATANABE, M. (1994): Influence of transition-metal type and content on local-order properties of $Zn_{1-x}M_xS$ (*M* = Mn,Fe,Co) alloys studied using XANES spectroscopy. *Phys. Rev. B* **50**, 7371-7377.

QIAN, J., SKYLLBERG, U., FRECH, W., BLEAM, W.F., BLOOM, P.R. & PETIT, P.E. (2002): Bonding of methyl mercury to reduced sulfur groups in soil and stream organic matter as determined by X-ray absorption spectroscopy and binding affinity studies. *Geochim. Cosmochim. Acta* **66**, 3873-3885.

RAYBAUD, P., HAFNER, J., KRESSE, G. & TOULHOAT, H. (1997): *Ab initio* density functional studies of transition-metal sulphides. II. Electronic structure. *J. Phys: Condensed Matter* **9**, 11107-11140.

REINEN, D. & LINDNER, G.-G. (1999): The nature of the chalcogen colour centres in ultramarine-type solids. *Chem. Soc. Rev.* **28**, 75-84.

SAINCTAVIT, P., PETIAU, J., CALAS, G., BENFATTO, M. & NATOLI, C.R. (1987): XANES study of sulfur and zinc K-edges in zincblende: experiments and multiple-scattering calculations. *J. Physique* **48**, C9-1109-C9-1112.

SAKKOPOULOS, S., VITORATOS, E. & ARGYREAS, T. (1984): Energy-band diagram for pyrrhotite. *J. Phys. Chem. Solids* **45**, 923-928.

_____, _____ & _____ (1986): Correlation between chemical bonds and properties in pyrrhotite. *J. Chem. Educ.* **63**, 665-666.

SARRET, G., CONNAN, J., KASRAI, M., BANCROFT, G.M., CHARRIÉ-DUHAUT, A., LEMOINE, S., ADAM, P., ALBRECHT, P. & EYBERT-BÉRARD, L. (1999): Chemical forms of sulfur in geological and archeological asphaltanes from Middle East, France, and Spain determined by sulfur *K*- and *L*-edge X-ray absorption near-edge structure spectroscopy. *Geochim. Cosmochim. Acta* **63**, 3767-3779.

_____, MONGENOT, T., CONNAN, J., DERENNE, S., KASRAI, M., BANCROFT, G.M. & LARGEAU, C. (2002): Sulfur speciation in kerogens of the Orbagnoux deposit (Upper Kimmeridgian, Jura) by XANES spectroscopy and pyrolysis. *Organic Geochem.* **33**, 877-895.

SATO, H., MIHARA, T., FURUTA, A., TAMURA, M., MIMURA, K., HAPPO, N., TANIGUCHI, M. & UEDA, Y. (1997): Chemical trend of occupied and unoccupied Mn 3*d* states in MnY (Y=S, Se,Te). *Phys. Rev. B* **56**, 7222-7231.

SCHIDLOWSKI, M. (1981): Uraniferous constituents of the Witwatersrand conglomerates: ore-microscopic observations and implications for the Witwatersrand metallogeny. *U.S. Geol. Surv., Prof. Pap.* **1161-N**, N1-N29.

SETTE, F., STÖHR, J. & HITCHCOCK, A.P. (1984): Correlation between intramolecular bond lengths and K-shell σ-shape resonances in gas-phase molecules. *Chem. Phys. Lett.* **110**, 517-520.

SKINNER, B.J. & LUCE, F.D. (1971): Solid solutions of the type (Ca,Mg,Mn,Fe)S and their use as geothermometers for the enstatite chondrites. *Am. Mineral.* **56**, 1269-1296.

SMART, R.ST.C., SKINNER, W.M. & GERSON, A.R. (1999): XPS of sulphide mineral surfaces: metal-deficient, polysulphides, defects and elemental sulphur. *Surface Interface Anal.* **28**, 101-105.

SOLDATOV, A.V., KRAVTSOVA, A.N., FLEET, M.E. & HARMER, S.L. (2004): Electronic structure of MeS (Me = Ni, Co, Fe): X-ray absorption analysis. *J. Phys.: Condensed Matter* **16**, 7545-7556.

SOLOMON, D., LEHMANN, J. & MARTÍN, C.E. (2003): Sulfur K-edge XANES spectroscopy as a tool for understanding sulfur dynamics in soil organic matter. *Soil Sci. Soc. Am. J.* **67**, 1721-1731.

SPIRO, C.L., WONG, J., LYTLE, F.W., GREGOR, R.B., MAYLOTTE, D.H. & LAMSON, S.H. (1984): X-ray absorption spectroscopic investigation of sulfur sites in coal: organic sulfur identification. *Science* **226**, 48-50.

STERN, E.A. (1988) Theory of EXAFS. *In* X-ray Absorption: Principles, Applications and Techniques of EXAFS, SEXAFS and XANES. Chemical Analysis, Vol. **92** (D.C. Koningsberger & R. Prins, eds.), John Wiley & Sons, New York, N.Y. (3-51).

STÖHR, J., GLAND, J.L., EBERHARDT, W., OUTKA, D., MADIX, R.J., SETTE, F., KOESTNER, R.J. & DOEBLER, U. (1983): Bonding and bond lengths of chemisorbed molecules from near-edge X-ray-absorption fine-structure studies. *Phys. Rev. Lett.* **51**, 2414-2417.

TAN, K.H., BANCROFT, G.M., COATSWORTH, L.L. & YATES, B.W. (1982): Mark IV "Grasshopper" grazing incidence monochromator for the Canadian Synchrotron Radiation Facility (CSRF). *Can. J. Phys.* **60**, 131-136.

TAYLOR, D. (1967): The sodalite group of minerals. *Contrib. Mineral. Petrol.* **16**, 172-188.

TOSSELL, J.A. (1977): SCF–Xα scattered wave MO studies of the electronic structure of ferrous iron in octahedral coordination with sulfur. *J. Chem. Phys.* **66**, 5712-5719.

_____ & VAUGHAN, D.J. (1992) *Theoretical Geochemistry: Applications of Quantum Mechanics in the Earth and Mineral Sciences*. Oxford University Press, New York, N.Y.

VAIRAVAMURTHY, A. (1998): Using X-ray absorption to probe sulfur oxidation states in complex molecules. *Spectrochim. Acta A* **54**, 2009-2017.

_____, MALETIC, D., WANG, S., MANOWITZ, B., EGLINTON, T. & LYONS, T. (1997): Characterization of sulfur-containing functional groups in sedimentary humic substances by X-ray absorption near-edge structure spectroscopy. *Energy Fuels* **11**, 546-553.

_____, MANOWITZ, B., LUTHER, G.W., III & JEON, Y. (1993a): Oxidation states of sulfur in thiosulfate and implications for anaerobic energy metabolism. *Geochim. Cosmochim. Acta* **57**, 1619-1623.

_____, _____, ZHOU, W. & JEON, Y. (1993b): Determination of hydrogen sulfide oxidation products by sulfur K-edge X-ray absorption near-edge structure spectroscopy. *In* Environmental Geochemistry of Sulfide Oxidation (C.N. Alpers & D.W. Blowes, eds.). *Am. Chem. Soc., Symp. Ser.* **550**, 412-430.

_____, ZHOU, WEIQING, EGLINTON, T. & MANOWITZ, B. (1994): Sulfonates: a novel class of organic sulfur compounds in marine sediments. *Geochim. Cosmochim. Acta* **58**, 4681-4687.

WALDO, G.S., CARLSON, R.M.K., MOLDOWAN, J.M., PETERS, K.E. & PENNER-HAHN, J.E. (1991): Sulfur speciation in heavy petroleums: information from X-ray absorption near-edge structure. *Geochim. Cosmochim. Acta* **55**, 801-814.

WOMES, M., KARNATAK, R.C., ESTEVA, J.M., LEFEBVRE, I., ALLAN, G., OLIVIER-FOURCADE, J. & JUMAS, J.C. (1997): Electronic structures of FeS and FeS_2: X-ray absorption spectroscopy and band structure calculations. *J. Phys. Chem. Solids* **58**, 345-352.

WU, Z.Y., OUVRARD, G. & NATOLI, C.R. (1997): Study of pre-edge structures in the K-edge XANES/ELNES spectra of some transition-metal oxides and sulfides. *J. de Physique France IV* **7**, C2-199-C2-201.

YANG, B.X., MIDDLETON, F.H., OLSSON, B.G., BANCROFT, G.M., CHEN, J.M., SHAM, T.K.,TAN, K. & WALLACE, D.J. (1992): The design and performance of a soft X-ray double crystal monochromator beamline at Aladdin. *Nucl. Instrum. Methods Phys. Res. A* **316**, 422-436.

ZAJDEL, P., KISIEL, A., ZIMNAL-STARNAWSKA, M., LEE, P.M., BOSCHERINI, F. & GIRIAT, W. (1999): XANES study of sulphur K edges of transition metal (V, Cr, Mn, Fe, Co, Ni) monosulphides: experiment and LMTO numerical calculations. *J. Alloys Compounds* **286**, 66-70.

Received December 23, 2004, revised manuscript accepted March 28, 2005.